

UNIVERSITY OF CALIFORNIA  
SANTA CRUZ

**A METAMODELING APPROACH FOR BIAS ESTIMATION OF  
BIOLOGICAL REFERENCE POINTS**

A dissertation submitted in partial satisfaction of the  
requirements for the degree of

DOCTOR OF PHILOSOPHY

in

STATISTICAL SCIENCE

by

**Nicholas Grunloh**

June 2024

The Dissertation of Nicholas Grunloh  
is approved:

---

Professor Herbert Lee, Chair

---

Edward J. Dick Ph.D.

---

Professor Paul Parker

---

Professor Bruno Sanso

---

Dean Peter F. Biehl  
Vice Provost and Dean of Graduate Studies

Copyright © by  
Nicholas Grunloh  
2024

# **Table of Contents**

# List of Figures

## Abstract

A Metamodeling Approach for Bias estimation of Biological Reference Points

by

Nicholas Grunloh

Stock assessments often assume a two-parameter functional form (e.g., Beverton-Holt or Ricker) for the expected recruitment produced by a given level of spawning output. Mangel et al. [?] and others have shown that biological reference points such as  $\frac{F^*}{M}$  and  $\frac{B^*}{\bar{B}(0)}$  are largely determined by a single parameter (steepness) when using two-parameter relationships. These functions introduce strong correlations between reference points (RP) that are pre-determined by the functional form, rather than a biological characteristic of the stock. Mangel et al. note that use of a three-parameter stock-recruitment relationship allows for independent estimation of these reference points. This research seeks to understand the nature of biases in reference points resulting from fitting a two-parameter logistic functional form when the true relationship follows a three-parameter stock-recruitment relationship (SRR). This work demonstrates the useful limits of the misspecified Schaefer model, and the mechanisms of model failure which arise from mapping a three-dimensional parameter space into two dimensions.

To myself,  
Perry H. Disdainful,  
the only person worthy of my company.

## **Acknowledgments**

I want to “thank” my committee, without whose ridiculous demands, I would have graduated so, so, very much faster.

# <sup>1</sup> **Chapter 1**

## <sup>2</sup> **Introduction**



### 3      *Generalize beyond production model*

4  
5      The most fundamental model in modern fisheries management is the surplus-production  
6 model. These models focus on modeling population growth via nonlinear paramet-  
7 ric ordinary differential equations (ODE). Key management quantities called reference  
8 points (RPs) are commonly derived from the ODE equilibrium equations and depend  
9 upon the parameterization of biomass production. Two-parameter forms of the produc-  
10 tion function have been shown to limit the theoretical domain of RPs [?]. The limited  
11 RP-space of two-parameter models makes these models vulnerable to model misspec-  
12 ification with respect to RPs, and thus the limiting structure of two-parameter models  
13 may in and of itself induce bias in RP estimation using these models. The behavior of  
14 RP estimation is not well understood and as a result patterns of bias in RP estimation  
15 may easily go unnoticed. A metamodeling approach is developed here to describe RP  
16 biases and explore mechanisms of model failure under the most common two-parameter  
17 models.

18      Data for a typical surplus-production model comes in the form of an index of abun-  
19 dance through time which is assumed to be proportional to the reproducing biomass  
20 for the modelled population that is vulnerable to fishing. The index is often observed  
21 alongside a variety of other known quantities, but at a minimum, each index will be  
22 observed in the presence of some known catch for the period. Figure (1.1) shows the  
23 classic Namibian Hake dataset [?, ?, ?] exemplifying the form.

Indices are assumed to have multiplicative log-normal errors, and thus the following  
observation model arises naturally,

$$I_t = qB_t e^{\varepsilon} \quad \varepsilon \sim N(0, \sigma^2). \quad (1.1)$$

24      Above  $q$  is often referred to as the “catchability parameter”; it serves as the propor-

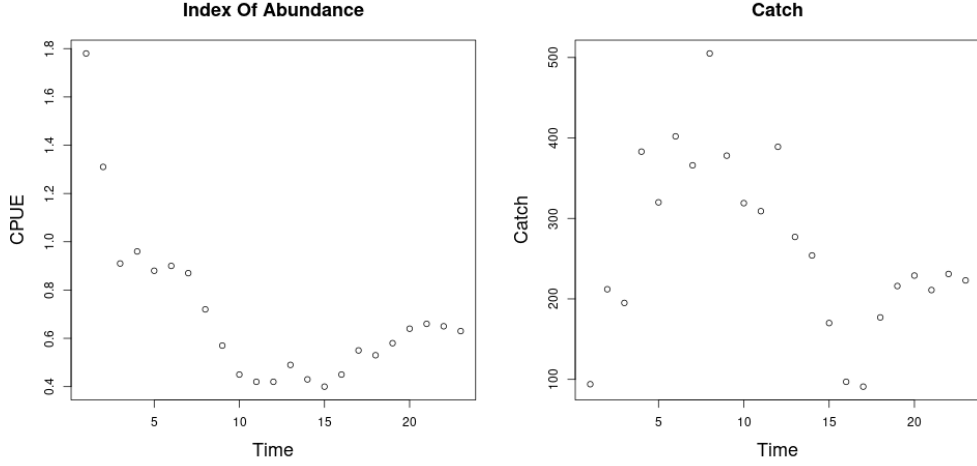


Figure 1.1: *left*: An index of abundance data, catch per unit effort (CPUE), for Namibian Hake from 1965 to 1987. *right*: The associated catch data for Namibian Hake over the same time period.

tionality constant mapping between the observed index of abundance and biomass.  $\sigma^2$  models residual variation. Biologically speaking  $q$  and  $\sigma^2$  are often treated as nuisance parameters with the “biological parameters” entering the model through a process model on biomass.

Biomass is assumed to evolve as an ODE; in this case I focus on the following form

$$\frac{dB}{dt} = P(B(t); \theta) - Z(t)B(t). \quad (1.2)$$

Here biomass is assumed to change in time by two processes, net production of biomass into the population,  $P(B)$ , and various sources of biomass removal,  $Z$ , from the population.

Firstly, the population grows through a production function,  $P(B)$ . Production in this setting is defined as the net biomass increase due to all reproduction and maturation processes. The production function is assumed to be a parametric (generally non-linear) function relating the current biomass of the population to an aggregate production of

37 biomass.

38 Secondly, the population decreases as biomass is removed by various sources that  
39 are assumed to remove biomass linearly with biomass. Above,  $Z(t)$ , is an aggregate  
40 rate of removal. When the fishing rate,  $F(t)$ , is the only source of removal  $Z(t) = F(t)$ ,  
41 however some models will also included other linear terms in  $Z(t)$ . Commonly the rate  
42 of “natural mortality”,  $M$ , is also included as an additional term so that  $Z(t) = M + F(t)$ .

43 From a management perspective a major goal of modeling is to accurately infer  
44 a quantity known as *maximum sustainable yield* (MSY). One could maximize simple  
45 yield at a particular moment in time (and only for that moment) by fishing all available  
46 biomass in that moment. This strategy is penny-wise but pound-foolish (not to mention  
47 ecologically devastating) since it doesn’t leave biomass in the population to reproduce  
48 in the future. We seek to fish in a way that allows (or even encourages) future produc-  
49 tivity in the population. This is accomplished by maximizing the equilibrium level of  
50 catch over time. Equilibrium yield is considered by replacing the steady state biomass  
51 ( $\bar{B}$ ) in the assumed form for catch, so that  $\bar{Y} = F\bar{B}(F)$ , where  $\bar{\phantom{x}}$  indicates a value at  
52 steady state. MSY is found by maximizing  $\bar{Y}(F)$  with respect to  $F$ , and  $F^*$  is the fish-  
53 ing rate at MSY. Going forward let  $*$  decorate any value derived under the condition of  
54 MSY.

55 Fisheries are very often managed based upon reference points which serve as sim-  
56 plified heuristic measures of population behavior. The mathematical form of RPs de-  
57 pends upon the model assumptions through the production function. While a number  
58 of different RPs exist which describe the population in different (but related) ways, the  
59 most common RPs revolve around the concept of MSY (or robust ways of measuring  
60 MSY [?, ?]). Here the focus is primarily on the RPs  $\frac{B^*}{\bar{B}(0)}$  and  $F^*$  ( $\frac{F^*}{M}$  when appropriate)  
61 for their pervasive use in modern fisheries [?].

62  $F^*$  is the afore mentioned fishing rate which results in MSY.  $\frac{B^*}{\bar{B}(0)}$  is the depletion  
63 of the stock at MSY. That is to say  $\frac{B^*}{\bar{B}(0)}$  describes the fraction of the unfished popu-

64 lation biomass that will remain in the equilibrium at MSY. In general  $F^* \in \mathbb{R}^+$  and  
65  $\frac{B^*}{B(0)} \in (0, 1)$ , however under the assumption of two-parameter production, models will  
66 be structurally unable to capture the full theoretical range of RPs.

67 Many of the most commonly used production functions depend only on two-parameters.  
68 For example, the Schaefer model depends only on the biological parameters  $r$  and  $K$ ,  
69 and limits RP inference so that under the Schaefer model  $\left(F^*, \frac{B^*}{B(0)}\right) \in (\mathbb{R}^+, \frac{1}{2})$ . The  
70 two-parameter Fox model [?] limits  $\left(F^*, \frac{B^*}{B(0)}\right) \in (\mathbb{R}^+, \frac{1}{e})$ . Similarly the two-parameter  
71 Cushing [?], Beverton-Holt [?, BH] and Ricker [?] production functions do not model  
72 the full theoretical space of RPs [?, ?].

73 The bias-variance trade-off [?] makes it clear that the addition of a third parameter  
74 in the production function will necessarily reduce estimation bias. However the utility  
75 of this bias reduction is still under debate because the particular mechanisms and be-  
76 havior (direction and magnitude) of these biases for key management quantities are not  
77 fully understood or described. Lee et al. [?] provides some evidence that estimation  
78 of productivity parameters are dependent on changes in biomass trend through time  
79 (i.e. contrast) as well as model specification. Conn et al. [?] comes to similar conclu-  
80 sions via calibration modeling techniques. These studies indicate important factors that  
81 contribute to inferential failure. However they do not offer mechanisms of model fail-  
82 ure, nor do their experimental designs allow for the control of different types of model  
83 misspecification.

84 In this study I consider the behavior of inference when index data are simulated  
85 from three-parameter PT and Schnute production models, but the simulated data are fit  
86 using intentionally misspecified two-parameter logistic or BH production models. The  
87 work begins with a derivation of RPs under the three-parameter models. A method is  
88 then presented for generating simulation designs based on the parametric form of RPs  
89 which serves as a control on the nature of simulated model misspecification. Finally a  
90 Gaussian Process (GP) metamodel [?] is constructed for exploration and analysis of RP

91 biases.

92     A key insight of this approach is that bias is considered broadly across RP-space to  
93 uncover patterns and correlations between RPs. The GP metamodel is explicit about  
94 trade-offs between RPs so as to inform the full utility of reducing bias, as well as to  
95 suggest mechanisms for understanding what causes bias. Further, the effect of contrast  
96 on estimation is considered together with model misspecification.

## <sup>97</sup> **Chapter 2**

### <sup>98</sup> **Pella-Tomlinson Model**

## 99 2.1 Introduction

## 100 2.2 Methods

### 101 2.2.1 Model

The three-parameter Pella-Tomlinson (PT) family has a convenient form that includes, among others [?, ?], the logistic production function as a special case. PT production function is parameterized so that  $\theta = [r, K, \gamma]$  and the family takes the following form,

$$P_p(B; [r, K, \gamma]) = \frac{rB}{\gamma - 1} \left( 1 - \left( \frac{B}{K} \right)^{(\gamma-1)} \right). \quad (2.1)$$

102  $\gamma$  is a parameter which breaks PT out of  
 103 the restrictive symmetry of the logistic curve.  
 104 In general  $\gamma \in (1, \infty)$ , with the logistic model  
 105 appearing in the special case of  $\gamma = 2$ , and  
 106 the Fox model appearing as a limiting case as  
 107  $\gamma \rightarrow 1$ . The parameter  $r$  controls the maxi-  
 108 mum per-capita growth rate of the population  
 109 in the absence of competition for resources  
 110 (i.e. the slope of production function at the  
 111 origin).  $K$  is the so called "carrying capac-  
 112 ity" of the population. In this context the  
 113 carrying capacity can be formally stated as  
 114 steady state biomass in the absence of fishing  
 115 (i.e.  $\bar{B}(0) = K$ ). In Figure (2.1) PT production  
 116 is shown for a range of parameter values so as

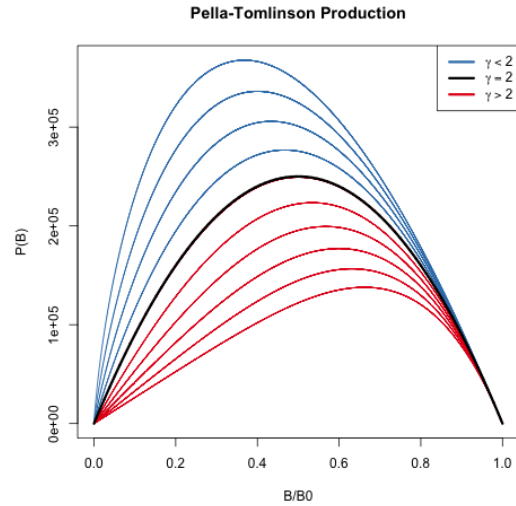


Figure 2.1: The Pella-Tomlinson production function plotted across a variety of parameter values. The special cases of Logistic production is shown in black, and the left-leaning and right-leaning regimes are shown in blue and red respectively.

117 to demonstrate the various productivity shapes that can be achieved under PT.

118 While the form of the PT curve produces some limitations [?], importantly the  
 119 introduction of a third parameter allows enough flexibility to fully describe the space of  
 120 reference points used in management. To see this, the reference points are analytically  
 121 derived for the PT model below.

## 122 2.2.2 Reference Points

123 With  $B(t)$  representing biomass at time  $t$ , under PT production, the dynamics of  
 124 biomass are defined by the following ODE,

$$\frac{dB}{dt} = \frac{rB}{\gamma-1} \left( 1 - \left( \frac{B}{K} \right)^{\gamma-1} \right) - FB. \quad (2.2)$$

An expression for the equilibrium biomass is attained by setting Eq (2.2) equal to zero, and rearranging the resulting equation to solve for  $B$ . Thinking of the result as a function of  $F$  gives,

$$\bar{B}(F) = K \left( 1 - \frac{F(\gamma-1)}{r} \right)^{\frac{1}{(\gamma-1)}}. \quad (2.3)$$

125 At this point it is convenient to notice that  $\bar{B}(0) = K$ . The expression for  $B^*$  is given  
 126 by evaluating Eq (2.3) at  $F^*$ . To get an expression for  $F^*$ , the equilibrium yield is  
 127 maximized with respect to  $F$ ,

$$F^* = \operatorname{argmax}_F F \bar{B}(F). \quad (2.4)$$

In the case of PT production this maximization can be done analytically, by differenti-



ating the equilibrium yield with respect to  $F$  as follows,

$$\frac{d\bar{Y}}{dF} = \bar{B}(F) + F \frac{d\bar{B}}{dF} \quad (2.5)$$

$$\frac{d\bar{B}}{dF} = -\frac{K}{r} \left( 1 - \frac{F(\gamma-1)}{r} \right)^{\frac{1}{\gamma-1}-1}. \quad (2.6)$$

Setting Eq (2.5) equal to 0, substituting  $\bar{B}(F)$  and  $\frac{d\bar{B}}{dF}$  by Equations (2.3) and (2.6) respectively, and solving for  $F$  produces the following expression for the fishing rate required to produce MSY,

$$F^* = \frac{r}{\gamma} \quad (2.7)$$

Plugging the above expression for  $F^*$  back into Eq (2.3) gives the following expression for biomass at MSY,

$$B^* = K \left( \frac{1}{\gamma} \right)^{\frac{1}{\gamma-1}}. \quad (2.8)$$

The above derived expressions for  $\bar{B}(0)$ ,  $B^*$ , and  $F^*$  can then be used to build a specific analytical form for the biological reference points in terms of only productivity parameters.

$$F^* = \frac{r}{\gamma} \quad \frac{B^*}{\bar{B}(0)} = \left( \frac{1}{\gamma} \right)^{\frac{1}{\gamma-1}} \quad (2.9)$$

### 128 2.2.3 Simulation

Generating simulated indices of abundance from the PT model requires inverting the relationship between  $\left( F^*, \frac{B^*}{\bar{B}(0)} \right)$ , and  $(r, \gamma)$ . It is not generally possible to analytically invert this relationship for many three-parameter production functions [?, ?]. Most three-parameter production functions lead to RPs that require expensive numeri-

cal methods to invert; more over the numerical inversion procedure can often be unstable. That said, for the case of PT this relationship is analytically invertible, and leads to the following relationship

$$r = \gamma F^* \quad \gamma = \frac{W\left(\frac{B^*}{\bar{B}(0)} \log\left(\frac{B^*}{\bar{B}(0)}\right)\right)}{\log\left(\frac{B^*}{\bar{B}(0)}\right)}. \quad (2.10)$$

129 Above  $W$  is the Lambert product logarithm function. More details about this derivation,  
130 and the Lambert product logarithm, are given in Appendix (??).

131 Using Eq. (2.10) to obtain production parameters, a PT production model can be  
132 fully defined for any combination of the RPs  $F^*$  and  $\frac{B^*}{\bar{B}(0)}$ . Since  $K$  does not enter the  
133 RP calculation its value is fixed arbitrarily at 10000.

134 Indices of abundance are simulated from the three-parameter PT production model  
135 broadly over the space of  $F^*$  and  $\frac{B^*}{\bar{B}(0)}$  via a space filling design as described in Section  
136 (3.2.3). A small amount of residual variation,  $\sigma = 0.01$ , is added to the simulated index,  
137 and these data are then fit with a Schaefer model, at various degrees of misspecification,  
138 so as to observe the effect of productivity model misspecification upon RP inference.

#### 139 2.2.4 Design

140 Letting  $\mathcal{F}$  and  $\mathcal{B}$  be regular grids, of size  $n = 100$ , on  $F^* \in (0.1, 0.7)$  and  $\frac{B^*}{\bar{B}_0} \in (0.2, 0.6)$   
141 respectively, a LHS design of size 100 is collected among the cells produced by  $\mathcal{F} \times \mathcal{B}$ .

142 Each of the sampled LHS design locations represent a unique PT model with the  
143 sampled RP values. Since the relationship mapping RPs analytically to productivity  
144 parameters can be found for the PT model, LHS designs the the PT model are computed  
145 directly in RP space and Eq. (2.10) is used to map the sampled RP design locations to  
146 PT productivity parameters.

### 147 2.2.5 Gaussian Process Metamodel

148 At its core, a metamodel is simply a model of some mapping of inputs to out-  
149 puts (the mapping itself is typically defined by a computer model). By modeling the  
150 mapping with a statistical model (that explicitly defines the relevant features of the  
151 mapping) a metamodel defines a specific ontology for the mapping. By simulating ex-  
152 amples of the mapping, the inferential infrastructure of the statistical model is used to  
153 empirically learn an effective emulation of the mapping within the ontology defined by  
154 the statistical model. The predictive infrastructure of the statistical model is then use-  
155 ful as an approximate abstraction of the system itself to better understand the system  
156 through further data collection, cheap approximation of the mapping, and/or study of  
157 the mapping itself.

158 In this setting, the aim of metamodeling is to study how well RPs are inferred when  
159 typical two-parameter models of productivity (Logistic and BH) are misspecified for  
160 populations that are actually driven by more complicated dynamics. The simulation  
161 design,  $\mathbf{X}$ , provides a sample of different population dynamics that are driven by three-  
162 parameter production functions broadly in RP space. By simulating index of abundance  
163 data from the three parameter model, and fitting those data with the two-parameter pro-  
164 duction model, we observe particular instances of how well RPs are inferred at the  
165 given misspecification of the two-parameter model relative to the true three-parameter  
166 production model. By gathering all of the simulated instances of how RPs are inferred  
167 (under the two-parameter model), we form a set of example mappings to train a meta-  
168 model which represents the mapping of true RPs (under the three-parameter model) to  
169 estimates of RPs under the misspecified two-parameter production model. The meta-  
170 model is essentially a surrogate for inference under the misspecified two-parameter  
171 production model that controls for the specific degree of model misspecification.

172 A flexible GP model is assumed for the structure of the metamodel to describe  
173 the mapping of RPs under misspecified two-parameter models of productivity. A GP

174 is a stochastic process generalizing the multivariate normal distribution to an infinite  
 175 dimensional analog. GP models are often specified primarily through the choice of a  
 176 covariance (or correlation) function which defines the relationship between locations  
 177 in the input space. Typically correlation functions are specified so that points closely  
 178 related in space result in correlated effects in the model. In this setting the inputs to  
 179 the GP metamodel are the space of reference points which define the simulated three-  
 180 parameter production models.

While index of abundance data are generated from three-parameter models, at each design location of the simulation, fitting the restricted two-parameter model results in a maximum likelihood estimate (MLE; and associated estimation uncertainty) of each of the productivity parameters (i.e. Schaefer:[ $\log(r)$ ,  $\log(K)$ ], BH:[ $\log(\alpha)$ ,  $\log(\beta)$ ]). To simplify the specification of the metamodel, let  $\mathbf{y}$  be a vector collecting the fitted MLEs for one of the productivity parameters, and let  $\boldsymbol{\omega}$  be a vector of estimates of the estimator variances (via the inverted Fisher information) at each  $\mathbf{y}$ . Each of the fitted productivity parameter estimates are then modeled using independent instances of the following GP metamodel.

$$\begin{aligned}\mathbf{y} &= \beta_0 + \mathbf{X}\boldsymbol{\beta} + \mathbf{v} + \boldsymbol{\epsilon} \\ \mathbf{v} &\sim N_n(\mathbf{0}, \tau^2 \mathbf{R}_\ell) \\ \boldsymbol{\epsilon} &\sim N_n(\mathbf{0}, \boldsymbol{\omega}' \mathbf{I})\end{aligned}\tag{2.11}$$

181  $\mathbf{X}$  is the  $n \times 2$  LHS design matrix of RPs for each simulated three-parameter data  
 182 generating model as described in Section (3.2.4.1).  $\boldsymbol{\epsilon}$  models independent normally  
 183 distributed error, which provides an ideal mechanism for propagating uncertainty from  
 184 inference in the simulation step into the metamodel. By matching each  $y_i$  with an ob-  
 185 served  $\omega_i$  variance term,  $\boldsymbol{\epsilon}$  serves to down weight the influence of each  $y_i$  in proportion  
 186 to the inferred production model sampling distribution uncertainty. This has the ef-

187 fect of smoothing the GP model in a way similar to the nugget effect [?], although the  
 188 application here models this effect heterogeneously.

The term,  $\mathbf{v}$ , contains spatially correlated GP effects. The correlation matrix,  $\mathbf{R}_\ell$  describes how RPs close together in the simulation design are more correlated than those that are far away. This spatial effect is modeled with a squared exponential correlation function,

$$R(\mathbf{x}, \tilde{\mathbf{x}}) = \exp \left( \sum_{i=1}^2 \frac{-(x_i - \tilde{x}_i)^2}{2\ell_j^2} \right). \quad (2.12)$$

189  $R$  has an anisotropic separable form which allows for differing length scales,  $\ell_1$   
 190 and  $\ell_2$ , in the different RP axes. The flexibility to model correlations separately in  
 191 the different RP axes is key due to the differences in the extent of the RP domains  
 192 marginally. The metamodel parameters  $\beta_0$ ,  $\beta$ ,  $\tau^2$ ,  $\ell_1$  and  $\ell_2$  are fit via MLE against the  
 193 observations  $\mathbf{y}$ ,  $\mathbf{X}$ , and  $\omega$  from simulation fits.

194 Fitting the metamodel allows for a full predictive description of inference under the  
 195 misspecified restricted models. Predictive estimates are obtained via kriging [?]

$$\hat{y}(\mathbf{x}) = \beta_0 + \mathbf{x}\beta + \mathbf{r}(\mathbf{x})' \mathbf{R}_\ell^{-1} \left( \mathbf{y} - (\beta_0 + \mathbf{X}\beta) \right) \quad (2.13)$$

196  $\hat{y}(\mathbf{x})$  is the predicted value of the modeled productivity parameter MLE under the  
 197 two-parameter production model, when the index of abundance is generated from the  
 198 three-parameter production model at RP location  $\mathbf{x}$ .  $\mathbf{r}(\mathbf{x})$  is a vector-valued function of  
 199 correlation function evaluations for the predictive location  $\mathbf{x}$  against all observations in  
 200  $\mathbf{X}$  (i.e.  $\mathbf{r}(\mathbf{x}) = \mathbf{R}(\mathbf{x}, \mathbf{x}_i) \forall \mathbf{x}_i \in \mathbf{X}$ ).

201 While metamodeling occurs on the inferred productivity parameters of the restricted  
 202 production model, the metamodel can also be used to build estimates of major bio-  
 203 logical RPs. For the BH model the relevant transformations for relating productivity

parameters with RPs are given in Eqs. (3.5, 3.8) with  $\gamma$  fixed to -1; for the Schaefer model  $\hat{B}^* = \frac{\hat{K}}{2}$  and  $\hat{F}^* = \frac{\hat{r}}{2}$ . Applying the metamodel predictive surfaces on the scale of RP estimates allows for the quantification of estimation bias that is induced by fitting a misspecified two-parameter production model to indices of abundance generated under three-parameter productivity.

## 2.2.6 Catch

It is known that contrast in the observed index and catch time series can effect inference on the productivity parameters [?]. In this setting contrast refers to changes in the long term trends of index data. Figure (2.2, *right*) demonstrates an example of biomass that includes contrast induced by catch. It is not well understood how contrast may factor into inferential failure induced by model misspecification. Thus catch is parameterized so as to allow for a spectrum of possible contrast simulation settings.

Catch is parameterized so that  $F(t)$  can be controlled with respect to  $F^*$ . Recall that catch is assumed to be proportional to biomass, so that  $C(t) = F(t)B(t)$ . To control  $F(t)$  with respect to  $F^*$ ,  $C(t)$  is specified by defining the quantity  $\frac{F(t)}{F^*}$  as the relative fishing rate.  $B(t)$  is defined by the solution of the ODE, and  $F^*$  is defined by the biological parameters of the model. By defining  $\frac{F(t)}{F^*}$ , catch can then be written as  $C(t) = F^* \left( \frac{F(t)}{F^*} \right) B(t)$ .

Intuitively  $\frac{F(t)}{F^*}$  describes the fraction of  $F^*$  that  $F(t)$  is specified to for the current  $B(t)$ . When  $\frac{F(t)}{F^*} = 1$ ,  $F(t)$  will be held at  $F^*$ , and the solution of the ODE brings  $B(t)$  into equilibrium at  $B^*$ . When  $\frac{F(t)}{F^*}$  is held constant in time biomass comes to equilibrium as an exponential decay from  $K$  approaching  $B^*$ . When  $\frac{F(t)}{F^*} < 1$ ,  $F(t)$  is lower than  $F^*$  and  $B(t)$  is pushed toward  $\bar{B} > B^*$ . Contrarily, when  $\frac{F(t)}{F^*} > 1$ ,  $F(t)$  is higher than  $F^*$  and  $B(t)$  is pushed toward  $\bar{B} < B^*$ ; the precise values of  $\bar{B}$  can be calculated from the steady state biomass equations provided above and depend upon the specific form of the production function.

For the simulations presented here, a family of fishing behaviors are considered where the fishing rate accelerates as technology and fishing techniques improve rapidly until management practices are applied, which ultimately brings fishing into equilibrium at  $F^*$ . This is parameterized as three distinct phases, over a total of 45 units of time, with each phase lasting 15 time units. The specific form is given below.

$$\frac{F(t)}{F^*} = ae^{bt}\mathbf{1}_{0 \leq t < 15} + (d - ct)\mathbf{1}_{15 \leq t < 30} + \mathbf{1}_{30 \leq t \leq 45} \quad (2.14)$$

The first term of Eq (2.14) is an exponential increase in fishing, the second term is a linear decline in relative fishing as initial management practices are applied, and the third term,  $\mathbf{1}_{30 \leq t \leq 45}$ , simply holds the fishing rate at  $F^*$  there after. These three phases are controlled by the four parameters  $a$ ,  $b$ ,  $c$ , and  $d$ . By enforcing that the interface of the phases meet at  $\chi_{max}$  and 1 respectively the relative fishing series is reduced to a two-parameter family.

$$a = e^{\log(\chi_{max}) - 15b} \quad b = \frac{1}{t - 15} \log \left( \frac{\chi_{min}}{\chi_{max}} \right) \quad (2.15)$$

$$c = \frac{\chi_{max} - 1}{15 - 1} \quad d = 15c + \chi_{max} \quad (2.16)$$

230 By further specifying  $\chi_{max} = 1.6\%$  and  $\chi_{min} = 0.4\%$  the two-parameters  $\chi_{max}$ , and  $\chi_{min}$   
 231 can be reduced to the single parameter  $\chi$ . The tuning parameter  $\chi$  then singularly  
 232 controls contrast that appears in time series data.

233 When  $\chi = 0$ , the relative fishing rate is a constant at 1 to create a low contrast  
 234 simulation environment. As  $\chi$  increases Eq (2.14) induces more and more contrast in  
 235 the observed index and catch time series until  $\chi = 1$  which produces a high contrast  
 236 simulation environment. Figure (2.2) demonstrates a spectrum of contrast simulation  
 237 environments as well as the time series data they induce in the solution of the production  
 238 model ODE.

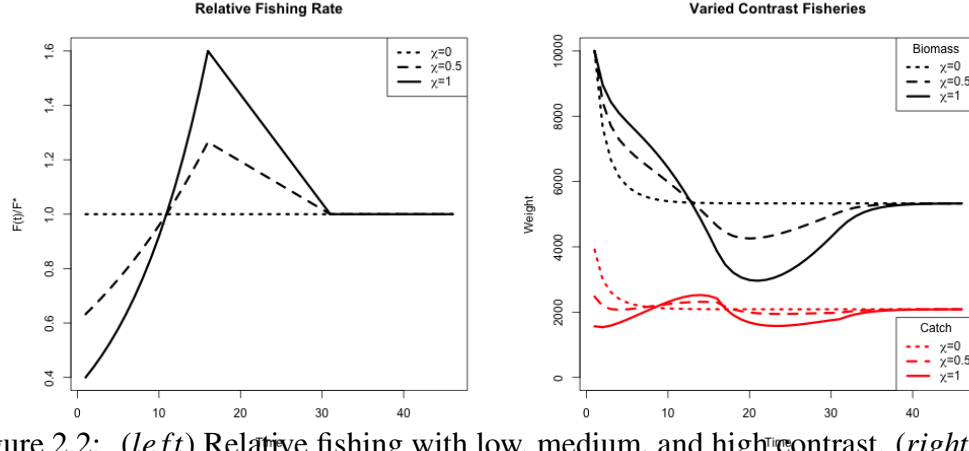


Figure 2.2: (left) Relative fishing with low, medium, and high contrast. (right) Population biomass and catch at each associated level of contrast.

### 2.2.7 Two-Parameter Production Model Inference

The simulated mapping results from fitting an intentionally misspecified two parameter production model to index of abundance data that are generated from a more complex three-parameter model of productivity. Thus, let  $I_t$  be an index of abundance simulated from the three-parameter PT or Schnute production models at time  $t \in \{1, 2, 3, \dots, T\}$ . However the fitted model is specified to be intentionally misspecified so that the fitted model is driven by a two-parameter Schaefer, or BH production model respectively.

The observation model for the fitted model is log-normal such that,

$$I_t | q, \sigma^2, \theta \sim LN(qB_t(\theta), \sigma^2). \quad (2.17)$$

$B_t(\theta)$  is defined by the solution of the ODEs defined by the Schaefer, or BH models. For the Schaefer model  $\theta = [r, K]$ , and for the BH model  $\theta = [\alpha, \beta]$ . From the perspective of the fitted model, the observed  $I_t$  are assumed independent conditional on  $q, \sigma^2, r, K$  and the two-parameter ODE model for biomass. Thus the log likelihood can be written



as

$$\log \mathcal{L}(q, \sigma^2, \theta; I) = -\frac{T}{2} \log(\sigma^2) - \frac{1}{2\sigma^2} \sum_t \log \left( \frac{I_t}{qB_t(\theta)} \right)^2. \quad (2.18)$$

247 In this setting,  $q$  is fixed at 0.0005 and  $M$  is fixed at 0.2, to focus on the inferential  
248 effects of model misspecification on biological parameters.  $\sigma^2$  and  $\theta$  are reparameter-  
249 ized to the log scale and fit via MLE. Reparameterizing the parameters to the log scale  
250 improves the reliability of optimization, in addition to facilitating the use of Hessian  
251 information for estimating MLE standard errors.

252 Given that the biological parameters enter the likelihood via a nonlinear ODE, and  
253 further the parameters themselves are related to each other nonlinearly, the likelihood  
254 function can often be difficult to optimize. A hybrid optimization scheme is used to  
255 maximize the log likelihood to ensure that a global MLE solution is found. The R pack-  
256 age GA [?, ?] is used to run a genetic algorithm to explore parameter space globally.  
257 Optimization periodically jumps into the L-BFGS-B local optimizer to refine optima  
258 within a local mode. The scheme functions by searching globally, with the genetic al-  
259 gorithm, across many initial values for starting the local gradient-based optimizer. The  
260 genetic algorithm serves to iteratively improve hot starts for the local gradient-based  
261 optimizer. Additionally, optimization is only considered to be converged when the op-  
262 timum results in an invertible Hessian at the found MLE.

### 263 2.2.8 Continuous model formulation

264 An important (and often overlooked) implementation detail is the solution to the  
265 ODE which defines the progression of biomass through time. As a statistical model it  
266 is of paramount importance that this ODE not only have a solution, but also that the  
267 solution be unique. Of primary concern, uniqueness of the ODE solution is necessary  
268 for well conditioned inference.

269 If the form of  $\frac{dB}{dt}$  is at least Lipschitz continuous, then the Cauchy-Lipschitz-Picard  
 270 theorem provides local existence and uniqueness of  $B(t)$ . Recall from Eq(1.2) that  $\frac{dB}{dt}$  is  
 271 separated into a term for biomass production,  $P(B)$ , and a term for removals,  $Z(t)B(t)$ .  
 272 For determining Lipschitz continuity of  $\frac{dB}{dt}$ , the smallest Lipschitz constant of  $\frac{dB}{dt}$  will  
 273 be the sum of the constants for each of the terms  $P(B)$  and  $Z(t)B(t)$  separately. Typ-  
 274 ically any choice of  $P(B)$  will be continuously differentiable, which implies Lipschitz  
 275 continuity. At a minimum  $Z(t)$  typically contains fishing mortality as a function of time  
 276  $F(t)$  to model catch in time as  $C(t) = F(t)B(t)$ .  $Z(t)$  may or may not contain  $M$ , but  
 277 typically  $M$  is modeled as stationary in time and does not pose a continuity issue, unlike  
 278 some potential assumptions for  $C(t)$ .

279 In practice  $C(t)$  is determined by a series of observed, assumed known, catches.  
 280 Catch observations are typically observed on a quarterly basis, but in practice may not  
 281 be complete for every quarter (or year) of the modeled period. It is overwhelmingly  
 282 common to discretize the ODE in time via Euler's method with integration step sizes  
 283 to match the observation frequency of the modeled data. This is often computationally  
 284 convenient when the underlying species dynamics are reasonably well behaved, however  
 285 when the dynamics model is used as a statistical model, with the goal of inferring  
 286 the behavior of the underlying species dynamics, the regularity of the dynamics are  
 287 not guaranteed. An implicit assumption of continuity of catch in time provides the  
 288 necessary regularity for the statistical model. Furthermore a continuous handling of  
 289 the dynamics provides improved accuracy in evaluating the ODE, particularly when  
 290 inferring productivity parameters which largely control the regularity of the dynamics.

291 While there are many ways to handle catch continuity, here I assume that catches  
 292 accrue linearly between observed catches. This assumption defines the catch function  
 293 as a piecewise linear function of time, with the smallest Lipschitz constant for the catch  
 294 term defined by the steepest time segment of the catch function. This assumption rep-  
 295 resents one of the simplest ways of handling catch, while retaining Lipschitz continuity

296 overall. Furthermore linearly interpolated catch is adequately parsimonious for the typ-  
297 ical handling of catches.

### 298 **2.2.8.1 Integration and Stiffness**

299 As previously mentioned, the overwhelming majority of implementations of stock  
300 assessment models discretized the ODE using Euler’s method with the integration step  
301 sized fixed so as to match the observation frequency. In this setting we explore model  
302 parameterizations that explore the full extent of biologically relevant reference points.  
303 This exercise produces some combinations of parameters that result in numerically stiff  
304 ODEs.

305 The concept of stiffness in ODEs is hard to precisely characterize. Hairer and Wan-  
306 ner [?, p.2] describe stiffness in the following pragmatic sense, “Stiff equations are  
307 problems for which explicit methods don’t work”. It is hard to make this definition  
308 more mathematically precise, but this a consistent issue for models of very productive  
309 species in the low contrast simulation. Euler’s method, as often implemented, is partic-  
310 ularly poorly suited for these stiff regions of parameter space. In these stiff regions it is  
311 necessary to integrate the ODE with an implicit integration method.

312 Several of the most common implicit methods were tried including the Livermore  
313 Solver for ODEs (lsode), and the Variable Coefficient ODE Solver (vode) as imple-  
314 mented in the deSolve package of R [?]. The difference between implicit solvers is  
315 negligible, while explicit methods result in wildly varying solutions to the ODE in stiff  
316 regions of parameter space. Results shown here are computed using the lsode inte-  
317 gration since it runs relatively quickly and has a relatively smaller footprint in system  
318 memory.

## 2.3 Results

### 2.3.1 An $MSY$ -Optimal Catch History

When  $F(t)$  is held constant at  $F^*$ , as it is in the “low contrast” simulation setting,  $B(t)$  comes to equilibrium as an exponential decay from  $K$  to  $B^*$ . Understanding model misspecification bias is simplified in this setting due to the relative simplicity that this induces in  $B(t)$ . However this simplicity is known to poorly inform estimates of  $r$ , and thus  $F^*$ , due to the limited range of the production function that is observed [?].

Figure (2.3) shows four of the most misspecified example production function fits as compared to the true data generating PT production functions. The rug plots below each set of curves show how the observed biomasses decay exponentially from  $K$  to  $B^*$  in each case. In particular, notice how observations only exist where the PT biomass is greater than  $B^*$ . Due to the leaning of the true PT curves, and the symmetry of the logistic parabola, the logistic curve only observes information about its slope at the origin from data observed on the right portion of the PT curves. The top two panels of Figure (2.3) shows PT data generated such that  $\frac{B^*}{B(0)} > 0.5$ ; in these cases PT is steeper to the right of  $B^*$  than it is on the left, and so the the logistic curve over-estimates  $r$ , and consequently also over-estimates  $F^*$ . The bottom two panels of Figure (2.3) show

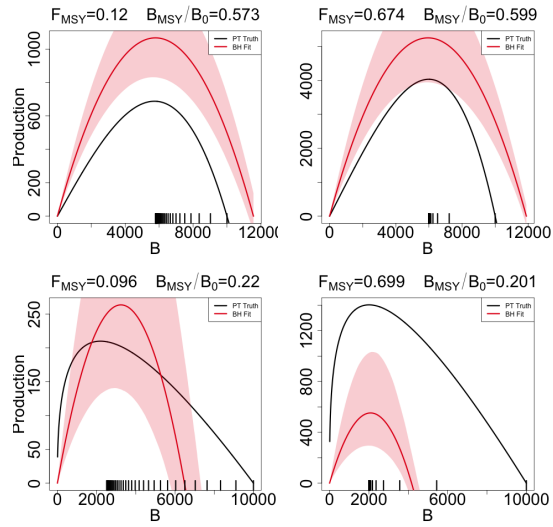


Figure 2.3: A comparison of the true PT production function (in black) and the estimated logistic curve (in red) with 95% CI shown. The examples shown represent the four corners of maximum model misspecification in the simulated RP-space. Observed biomasses are plotted in the rug plots below the curves.

PT data generated with  $\frac{B^*}{B(0)} < 0.5$  and where the vice versa phenomena occurs. PT is shallower to the right of  $B^*$  than it is on the left and so the logistic parabola estimate tends to under estimate  $F^*$ .

### 2.3.1.1 Metamodeled Trends

Each point in the space of the RPs  $F^*$  and  $\frac{B^*}{B(0)}$  uniquely identifies a complete PT model with different combinations of parameters values. Recall that when  $\gamma = 2$  for the PT model, the PT curve becomes a parabola and is equivalent to the logistic curve of the Schaefer model. Since the logistic curve is symmetric about  $B^*$ , the Schaefer model must fix the value of  $\frac{B^*}{B(0)}$  at the constant 0.5 for any value of  $F^*$ . So the line through RP space defined by  $\frac{B^*}{B(0)} = 0.5 \quad \forall F^*$ , defines the subset of RP space where  $\gamma = 2$  and where the PT model is equivalent to the Schaefer model. For brevity this subset of RP where  $\frac{B^*}{B(0)} = 0.5$  will be referred to as the ‘‘Schaefer set’’. Thus simulated data that are generated along the Schaefer set will be the only data that are not misspecified relative to the Schaefer model; as PT data are simulated farther and farther away from this line at  $\frac{B^*}{B(0)} = 0.5$  model misspecification of the Schaefer model becomes worse and worse.

While Figure (2.3) demonstrates a real trend in simulation results, individual simulation runs will at best show jittery trends due to the stochastic nature of statistical inference. The GP process metamodel accounts for this stochasticity to focus analysis on the signal in the simulation results. Recall that metamodeling occurs on the scale of the inferred productivity parameters of the restricted production model, by transforming metamodel predictions via Eq. (2.9), metamodeled predictions are obtained for Schaefer RPs. By further subtracting the true data generating PT RPs from the predicted Schaefer RPs at each point in RP space a pattern of inferential RP bias, induced by model misspecification of the Schaefer model, can be seen.

Figure (2.4) shows the pattern of biases the Schaefer model creates when fit to PT data generated at each point of RP space. An equivalent way to think of Figure

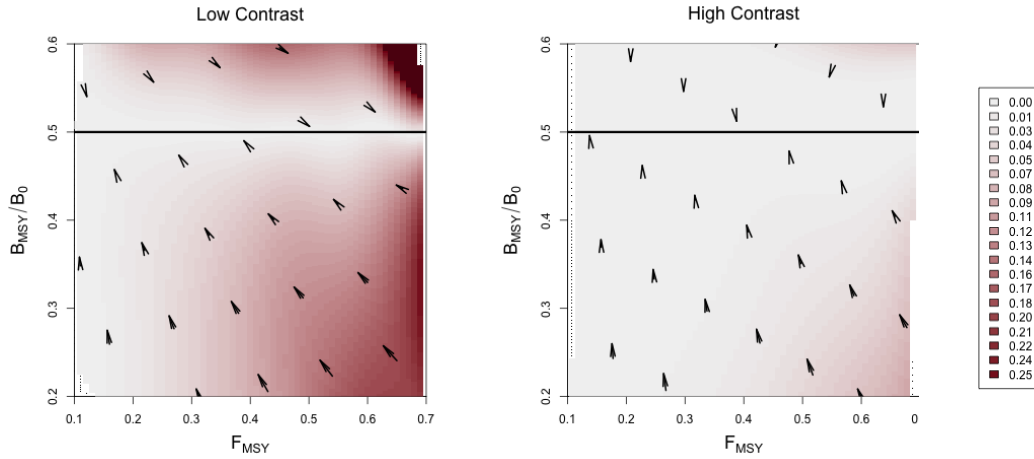


Figure 2.4: Joint bias direction for  $(F^*, \frac{B^*}{B_0})$  estimates under the misspecified Schaefer Model. The intensity of color represents the excess bias relative to the shortest possible mapping. Results in the low contrast setting are shown *left*, and the high contrast setting is shown *right*.

(2.4) is that since the Schaefer model must estimate RPs in the Schaefer set, the meta-model arrows indicate the mapping that is created by inferring RPs under a misspecified Schaefer model fit to PT data generated at each point over the pictured region.

Since  $\frac{B^*}{B_0}$  must be 0.5 under the Schaefer model, biases in the  $\frac{B^*}{B_0}$  direction must simply map vertically onto the Schaefer set. Due to this simplified RP geometry under the Schaefer model, the degree of bias in  $\frac{B^*}{B_0}$  estimation is defined solely by the degree of model misspecification irrespective of  $F^*$ . Furthermore, the closest possible point along the Schaefer set that Schaefer model inference could map RPs would be the perfectly vertical mapping. This pattern only contains the strictly necessary bias present in  $\frac{B^*}{B_0}$ , and zero bias in  $F^*$ . Any deviation from this minimal bias pattern is necessarily due to added bias in  $F^*$ .

The two simulation settings shown in Figure (2.4) are identical except for the amount of contrast present in the simulated index. The left panel of Figure (2.4) shows RP biases in the low contrast setting, while the right panel shows the high contrast setting.

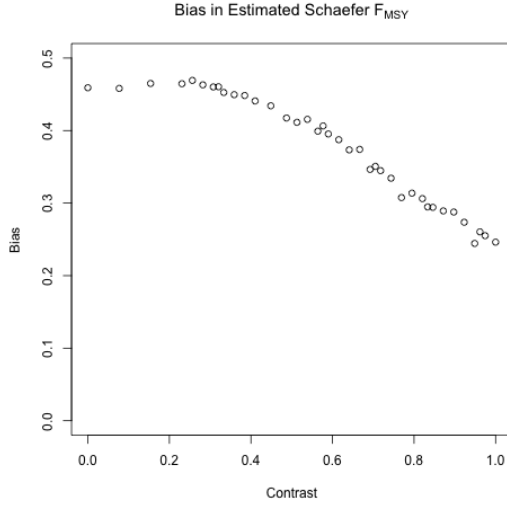


Figure 2.5: Bias in  $F^*$  under the Schaefer model when PT data are generated with increasing contrast so that  $F^*$  and  $\frac{B^*}{B_0}$  are fixed at 0.699 and 0.201 respectively.

385 Notice that in the low contrast setting the RP bias pattern is far from the minimum  
 386 distance mapping, however when contrast is added the mapping becomes much closer  
 387 to a minimal vertical bias mapping. In the low contrast setting the observed bias is  
 388 consistent with the pattern and mechanism described in Figure (2.3), where  $F^*$  is un-  
 389 derestimated for data generated below the Schaefer line and overestimated above the  
 390 Schaefer set. In the high contrast simulation the mapping is nearly minimal distance  
 391 with the exception of PT data generated with simultaneously low  $\frac{B^*}{B_0}$  and high  $F^*$ .

392 Figure (2.5) demonstrates how bias in  $F^*$  estimation decreases as contrast is added  
 393 to PT data as generated in the low  $\frac{B^*}{B_0}$  and high  $F^*$  regime. By including additional  
 394 contrast  $F^*$  bias is decreased, however parameterizing contrast so as to fully extinguish  
 395  $F^*$  bias may require a more complex model of fishing.

## 396 2.4 Discussion

397 *Tease Out BH*

398

399 Results presented here generally agree with what is known about estimating popu-

lation growth rate parameters [?, ?, ?]. These studies appreciate the role of contrast for estimating growth rates, however they struggle to make generally extensible conclusions since they focus only on a handful of stocks that fall short of forming a random sample of the greater population of possible stock behaviors. The LHS design methods presented here are designed specifically to simulate a representative sample of stocks broadly across the space of possible RPs. Furthermore, the simulation design, taken together with the GP metamodel of productivity parameter estimates, allows this study to control the degree of model misspecification and generalize conclusions about the behavior of productivity estimation within the production model setting presented.

In the presence of contrast,  $F^*$  estimation can enjoy very low bias even for a wide range of poorly specified models; conversely in the absence of contrast  $F^*$  estimation can suffer very large bias even for slightly misspecified models. This pattern is particularly true for low-contrast inference under the Schaefer model where the geometry of the restricted RP set isolates estimation failure of  $F^*$  from  $\frac{B^*}{B(0)}$ . While contrast has a similar impact on  $F^*$  estimation under the BH model, the geometry of the BH RP set correlates estimation bias of  $F^*$  and  $\frac{B^*}{B(0)}$ . The GP metamodeling approach reveals a more general pattern that highly informative data sets (high contrast) produces a nearly minimal distance mapping of RPs onto the constrained RP set.

In all cases when model misspecification is removed, even with weakly informative data, RP estimation is unbiased and well estimated. Thus contrast alone is not the only factor leading to inferential failure. Model misspecification is a necessary but not sufficient condition for inducing RP estimation bias. The particular RP bias present depends on the RP geometry of the fitted model and how that geometry is misspecified relative to the data. The RP mapping is then oriented to the RP geometry of the fitted model.

While the relative fishing rate parameterized in Section (2.2.6) captures a usefully broad spectrum of relevant fishing behaviors, it is still limiting in the amount of infor-



427 mation that it can induce. Improved methods for quantifying contrast in fisheries data,  
 428 and/or methods of discovering more informative fishing behavior, could improve this  
 429 analysis. In the absence of a maximally informative dataset simulation methods will not  
 430 fully describe how inference fails, but the methods presented here tell the most com-  
 431 plete picture yet, with explicit control of the degree model misspecification, contrast,  
 432 and a simulation design that allows for uniform representative data generation across  
 433 biologically meaningful stocks. The results presented here suggest the conjecture that  
 434 under a maximally informative dataset, RP inference with a two parameter production  
 435 function will be biased in the direction a shortest distance map from the true RPs onto  
 436 restricted set of RPs under the two-parameter model.

437 Given the potential for model misspecification of RPs, a minimal distance map-  
 438 ping of RPs represents a best-case scenario where the total bias of RPs, when mea-  
 439 sured jointly, is minimized. That said, without recognizing the geometry of how two-  
 440 parameter models of productivity limit RP space this may lead to unintuitive implica-  
 441 tions in RP estimation. For example, due to the shape of the BH RP set a minimal  
 442 distance mapping ensures that if there is bias in one of  $\frac{B^*}{B_0}$  or  $F^*$ , there will necessarily  
 443 be bias in the other RP. However under the Schaefer model, since the RP set is a con-  
 444 stant in  $\frac{B^*}{B_0}$ , bias in  $F^*$  is not adulterated in the same way by bias in  $\frac{B^*}{B_0}$  estimation. While  
 445 models with constant RPs, such as the logistic model  $\frac{B^*}{B_0} = \frac{1}{2}$  or the Fox model  $\frac{B^*}{B_0} = \frac{1}{e}$ ,  
 446 are extremely limited, they can be valuable tools for developing intuition precisely be-  
 447 cause they isolate RP estimation in their free RPs from the correlated RP biases present  
 448 in models like the BH or Ricker model.

449 When one considers the implications of RP bias, overestimation of RPs carries the  
 450 severe implication of management recommendations potentially leading to overfishing,  
 451 while underestimation of RP leads to overly conservative management. In this sense,  
 452 when the true model is not known, the geometry of the BH set together with the meta-  
 453 modeled bias trends makes the BH model a naturally conservative estimator of RPs for

454 most stocks. For most non-BH populations the BH model is likely to make conservative  
455 errors in its estimates of  $F^*$  and  $\frac{B^*}{B_0}$ . The one notable exception to the conservatism of  
456 the BH model stands for data generated in the Cushing-like regime of Schnute RPs. In  
457 this regime the BH model tends to be fairly unbiased overall, however the bias that is  
458 present for these populations tends to be overestimation in both RPs, leading to much  
459 more severe management consequences for those populations.

460 The RP bias trends of the Schaefer model demonstrate much less conservatism than  
461 the BH overall. For any population with  $\frac{B^*}{B_0} < 0.5$ ,  $\frac{B^*}{B_0}$  will be overestimated. When  
462 the population comes from the regime where  $\frac{B^*}{B_0} > 0.5$ ,  $\frac{B^*}{B_0}$  will be under estimated,  
463 but  $F^*$  is likely to be overestimated depending on the degree of contrast present in the  
464 data. So while the Schaefer model is an intuitive model, it tends to lead to much less  
465 conservative RP estimation.

466 While it is important to recognize these limitations of two-parameter models of  
467 productivity, we should not solely accept conservatism as a rationale of choosing a  
468 BH model of productivity. Increasing the flexibility of the production function by  
469 moving toward three-parameter models would release the underlying structural limi-  
470 tations [?] that cause these RP biases in the first place. Punt & Cope [?] considers a  
471 suite of possible three-parameter curves which could be used instead of current two-  
472 parameter curves. For all of their benefits, three parameter production functions have  
473 their own complicating factors, and the structure present in the Schnute model explored  
474 here makes it an intuitive bridge model for developing three-parameter models going  
475 forward.

## <sup>476</sup> **Chapter 3**

## <sup>477</sup> **Schnute Model**

## 3.1 Introduction

## 3.2 Methods

### 3.2.1 Model

The Schnute production function is a three-parameter generalization of many of the most common two-parameter production functions [?, ?]. It can be written in the following form, with parameters  $\alpha$ ,  $\beta$ , and  $\gamma$ ,

$$P_s(B; [\alpha, \beta, \gamma]) = \alpha B(1 - \beta\gamma B)^{\frac{1}{\gamma}}. \quad (3.1)$$

The BH and Logistic production functions arise when  $\gamma$  is fixed to -1 or 1 respectively. The Ricker model is a limiting case as  $\gamma \rightarrow 0$ . For  $\gamma < -1$  a family of strictly increasing Cushing-like curves arise, culminating in linear production as  $\gamma \rightarrow -\infty$ . These special cases form natural regimes of similarly behaving production functions as seen in Figure (3.1).

The behavior of RP inference under the BH model is of particular interest due to the overwhelming popularity of the BH assumption in fisheries models. Since

Schnute production models can represent a quantifiably wide variety of possible productivity behaviors, they present an ideal simulation environment for inquiry of the reliability of inference under the BH assumption.

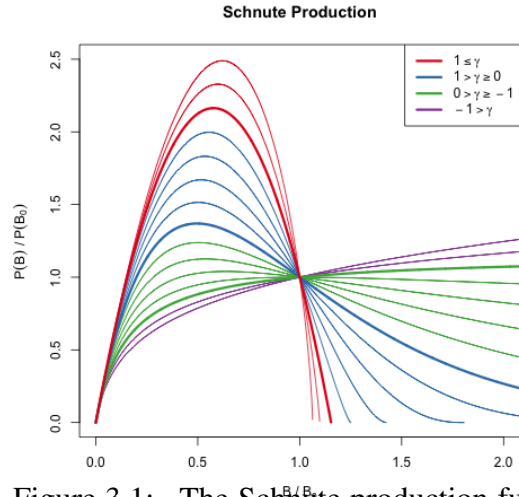


Figure 3.1: The Schnute production function plotted across a variety of parameter values. Regimes of similarly behaving curves are grouped by color.

Under Schnute production, biomass dynamics evolve according to the following ODE,

$$\frac{dB}{dt} = P_s(B; \theta) - (M + F)B. \quad (3.2)$$

497 This equation largely takes the same form as previously described, except that  $P_s$  is  
 498 the Schnute production function and natural mortality,  $M$ , is modeled explicitly here.  
 499 Natural mortality models the instantaneous rate of mortality from all causes outside of  
 500 fishing. While Eq. (3.2) models  $M$  explicitly, natural mortality is implicit to the struc-  
 501 ture of the previously decribed Schaefer, Fox, and PT production models. Explicitly  
 502 modeling natural mortality allows for the production function not to approach (or inter-  
 503 sect) 0 for large biomasses (e.g. BH production). In turn, the Schunte model requires  
 504 the addition of the term  $-MB$  to form an interpretable yeild curve and make RPs well  
 505 defined over the relevant domain of  $\gamma$ .

The derivation of RPs under Eq. (3.2) follows a similar logic as under the PT model. An expression for equilibrium biomass is attained by setting  $\frac{dB}{dt} = 0$  and rearranging the resulting expression to solve for  $B$

$$\bar{B}(F) = \frac{1}{\gamma\beta} \left( 1 - \left( \frac{M+F}{\alpha} \right)^\gamma \right). \quad (3.3)$$

The above expression quickly yields  $B_0$ ,  $B^*$  by evaluation at  $F = 0$  and  $F^*$  respectively,

$$B_0 = \frac{1}{\gamma\beta} \left( 1 - \left( \frac{M}{\alpha} \right)^\gamma \right) \quad (3.4)$$

$$\frac{B^*}{B_0} = \frac{1 - \left( \frac{M+F^*}{\alpha} \right)^\gamma}{1 - \left( \frac{M}{\alpha} \right)^\gamma}. \quad (3.5)$$

Attaining an expression for  $F^*$  requires maximization of equilibrium yield,  $\bar{Y} = F\bar{B}(F)$ ,

with respect to  $F$ . Analytically maximizing proceeds by differentiating  $\bar{Y}$  to produce

$$\frac{d\bar{Y}}{dF} = \bar{B}(F) + F \frac{d\bar{B}}{dF} \quad (3.6)$$

$$\frac{d\bar{B}}{dF} = -\frac{1}{\beta} \left( \frac{\left(\frac{M+F}{\alpha}\right)^\gamma}{F+M} \right). \quad (3.7)$$

Setting  $\frac{d\bar{Y}}{dF} = 0$ , filling in the expressions for  $\bar{B}(F)$  and  $\frac{d\bar{B}}{dF}$ , then rearranging to solve for  $F^*$  is less yielding here than it was in the case of the PT model. This procedure falls short of providing an analytical solution for  $F^*$  directly in terms of  $\theta$ , but rather shows that  $F^*$  must respect the following expression,

$$0 = \frac{1}{\gamma} - \left( \frac{1}{\gamma} + \frac{F^*}{F^* + M} \right) \left( \frac{F^* + M}{\alpha} \right)^\gamma. \quad (3.8)$$

506 The lack of an analytical solution here is understood. Schnute & Richards [?, pg.  
507 519] specifically point out that  $F^*$  cannot be expressed analytically in terms of pro-  
508 ductivity parameters, but rather gives a partial analytical expression for the inverse  
509 relationship. Although parameterized slightly differently, Schnute & Richards derive  
510 expressions for  $\alpha$  and  $\beta$  as a function of RPs and  $\gamma$ .

511 Since RPs are left without a closed form expression, computing RPs from produc-  
512 tivity parameters amounts to numerically solving the system formed by collecting the  
513 expressions (3.8), (3.4), and (3.5).

### 514 3.2.2 Simulation

515 For the purpose of simulation, it is not necessary to completely know the precise  
516 relationships mapping RPs  $\mapsto \theta$  or  $\theta \mapsto$  RPs. Simulation only requires enough knowl-  
517 edge of these mappings to gather a list of  $(\alpha, \beta, \gamma)$  tuples, for data generation under  
518 the Schnute model, and the corresponding RPs in some reasonable space-filling design

519 over RP space.

Similarly to Schnute & Richards [?], expressions (3.8) and (3.4) are solved for  $\alpha$  and  $\beta$  respectively. This leads to the partial mapping  $(F^*, B_0) \mapsto (\alpha(\cdot, \gamma), \beta(\cdot, \gamma))$  in terms of RPs and  $\gamma$ . By further working with Eq. (3.5), to identify  $\gamma$ , the following system is obtained,

$$\begin{aligned}\alpha &= (M + F^*) \left( 1 + \frac{\gamma F^*}{M + F^*} \right)^{1/\gamma} \\ \beta &= \frac{1}{\gamma B_0} \left( 1 - \left( \frac{M}{\alpha} \right)^\gamma \right) \\ \frac{B^*}{B_0} &= \frac{1 - \left( \frac{M + F^*}{\alpha} \right)^\gamma}{1 - \left( \frac{M}{\alpha} \right)^\gamma}.\end{aligned}\tag{3.9}$$

520 For a population experiencing natural mortality  $M$ , by fixing  $F^*$ ,  $B_0$ , and  $\frac{B^*}{B_0}$  the  
521 above system can fully specify  $\alpha$  and  $\beta$  for a given  $\gamma$ . Notice for a given  $\gamma$  a cascade  
522 of closed form solutions for  $\alpha$  and  $\beta$  can be obtained. First  $\alpha(\gamma)$  can be computed, and  
523 then  $\beta(\alpha(\gamma), \gamma)$  can be computed. If  $\alpha(\gamma)$  is filled back into the expression for  $\frac{B^*}{B_0}$ , the  
524 system collapses into a single onerous expression for  $\frac{B^*}{B_0}(\alpha(\gamma), \gamma)$ . For brevity, define  
525 the function  $\zeta(\gamma) = \frac{B^*}{B_0}(\alpha(\gamma), \gamma, F^*, M)$  based on Eq. (3.5).

526 Inverting  $\zeta(\gamma)$  for  $\gamma$ , and computing the cascade of  $\alpha(\gamma)$ , and then  $\beta(\alpha(\gamma), \gamma)$ , fully  
527 defines the Schnute model for a given  $(\frac{F^*}{M}, \frac{B^*}{B_0})$ . However inverting  $\zeta$  accurately is ex-  
528 tremely difficult. Inverting  $\zeta$  analytically is not feasible, and numerical methods for  
529 inverting  $\zeta$  are unstable and can be computationally expensive. Rather than numeri-  
530 cally invert precise values of  $\zeta(\gamma)$ ,  $\gamma$  is sampled so that the overall simulation design is  
531 space filling as described in Section (3.2.4).

532 Each design location defines a complete Schnute production model with the given  
533 RP values. Indices of abundance are simulated from the Schnute model at each design  
534 location, a small amount of residual variation,  $\sigma = 0.01$ , is added to the simulated index,

535 and the data are then fit with a misspecified BH production model. The design at large  
536 captures various degrees of model misspecification relative to the BH model, so as to  
537 observe the effect of productivity model misspecification upon RP inference.



### 3.2.3 Latin Hypercube Sampling

The goal of space filling design in this setting is to extend the notion of the random sample (and its desirable parameter estimation properties) across the simulated RP domain so as to represent the simulated space as well as possible [?]. The simple random sample is the classical approach to unbiased parameter estimation, however simple randomness is patchy, often sampling some regions of design space quite densely, while leaving other regions of design space empty. Space filling designs aim to preserve (or enhance) parameter estimation properties across the simulated domain [?, ?], while constraining samples to be spaced in some notion of spread over the entire space. Latin hypercube sampling [?, LHS] is among the most foundational of space filling designs used in computer experiments.

A LHS of size  $n$ , in the 2 dimensional space defined by RPs, distributes samples so as to spread points across a design region in a broadly representative way. A LHS design extends the notion of a univariate random uniform sample across multiple dimensions so that each margin of the design space enjoys a uniform distribution.

LHS designs achieve this notion of uniformity by first partitioning each dimension of the design space into regular grids of size  $n$ . By intersecting the grids

of each dimension, cells are produced that evenly partition the design space. In two dimensions  $n^2$  cells are produced, from which a total of  $n$  samples are taken. Crucially only one point is randomly sampled from a given element of each grid in each

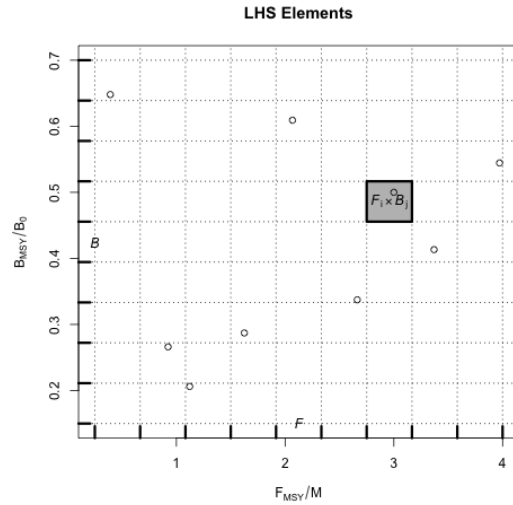


Figure 3.2: LHS grids. Intersecting  $\mathcal{F}$  and  $\mathcal{B}$  produces  $n^2$  cells; a particular cell  $\mathcal{F}_i \times \mathcal{B}_j$  is shown in grey. One point is in each of the marginal  $\mathcal{F}_i$  and  $\mathcal{B}_j$  grid elements.

565 dimension so as to reduce clumping of the  $n$  samples across the design space.

### 566 3.2.4 Design

567 Due to the lack of an analytical relationship mapping RPs  $\mapsto \theta$ , analogous to the PT  
 568 model's Eq. (2.10), producing a LHS design over Schnute RPs requires a more tactful  
 569 approach. The structured relationship between the RPs and productivity parameters,  
 570 described in Section (3.2.2), allows an approximate LHS to be obtained by a careful  
 571 navigation of the system of equations seen in Eq. (3.9).

572 Under the Schnute model, let  $\mathcal{F}$   
 573 and  $\mathcal{B}$  represent regular grids on  $\frac{F^*}{M} \in (0.25, 4)$  Given  $B_0$ ,  $M$ , and  $F^*$ :  
 574 and  $\frac{B^*}{B_0} \in (0.15, 0.7)$  respectively which 1) Draw  $\gamma^* \sim \gamma|F^*, M$ .  
 575 can serve as the scaffolding for comput- 2) Compute  $\frac{B^*}{B_0} = \zeta(\gamma^*)$   
 576 ing an approximate LHS. 3) Compute  $\alpha^* = \alpha(\gamma^*, F^*, M)$   
 4) Compute  $\beta^* = \beta(\alpha^*, \gamma^*, M, B_0)$

Since it is not practical to invert  $\zeta(\gamma)$ ,  
 a uniform sample in  $\frac{B^*}{B_0}$  can be obtained  
 by modeling  $\gamma$  as a random variable, with  
 realization  $\gamma^*$ , and thinking of  $\zeta(\gamma)$  as its  
 cumulative distribution function (CDF).

Figure 3.3: An outline of the sampling procedure for  $\gamma$  given  $B_0$ ,  $M$ , and  $F^*$ .

The aim is to model  $\gamma$  as an easily sampled random variable with a CDF that closely approximates  $\zeta$ , so that  $\zeta(\gamma^*) \sim U(\zeta_{min}, 1)$  as closely as possible. There may be many good models for the distribution of  $\gamma$ , but in this setting the following distribution is very effective,

$$\gamma \sim \zeta_{min} \delta(\gamma_{min}) + t(\mu, \sigma, v) \mathbf{1}_{\gamma > \gamma_{min}}. \quad (3.10)$$

577 Above,  $t$  is the density of the three-  
 578 parameter location-scale family Student's  
 579  $t$  distribution with location  $\mu$ , scale  $\sigma$ , and  
 580 degrees of freedom  $\nu$ .  $\mathbf{1}_{\gamma > \gamma_{min}}$  is an indi-  
 581 cator function that serves to truncate the  
 582 Student's  $t$  distribution at the lower bound  
 583  $\gamma_{min}$ .  $\delta(\gamma_{min})$  is the Dirac delta function  
 584 evaluated at  $\gamma_{min}$ , which is scaled by the  
 585 known value  $\zeta_{min}$ ; this places probability  
 586 mass  $\zeta_{min}$  at the point  $\gamma_{min}$ . Since sam-  
 587 pling from a Student's  $t$  distribution is  
 588 readily doable, sampling from a truncated  
 589 Student's  $t$  mixture only requires slight modification.

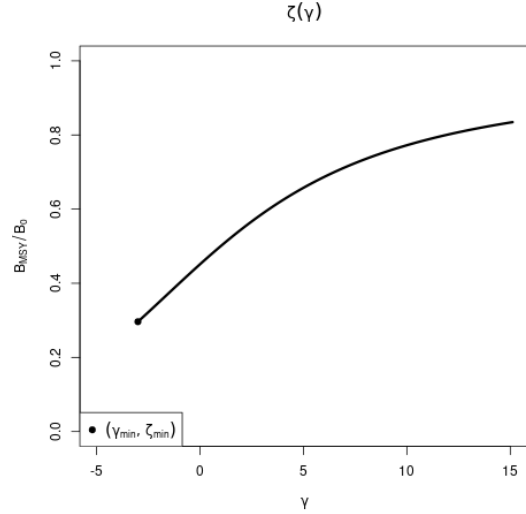


Figure 3.4:  $\zeta(\gamma)$  Plotted for  $F^* = 0.1$  and  $M = 0.2$ . The point  $(\gamma_{min}, \zeta_{min})$  shows the lowest biologically meaningful value of  $\gamma$ ; below which productivity is negative.

Let  $T$  be the CDF of the modeled distribution of  $\gamma$ . Since the point  $(\gamma_{min}, \zeta_{min})$  is known from the dynamics of the Schnute model at a given RP, full specification of Eq. (3.10) only requires determining the values for  $\mu$ ,  $\sigma$ , and  $\nu$  which make  $T$  best approximate  $\zeta(\gamma)$ . Thus, the values of  $\mu$ ,  $\sigma$ , and  $\nu$  are chosen by minimizing the  $L^2$  distance between  $T(\gamma)$  and  $\zeta(\gamma)$ .

$$[\hat{\mu}, \hat{\sigma}, \hat{\nu}] = \arg \min_{[\mu, \sigma, \nu]} \int_{\Gamma} (T(\gamma; \mu, \sigma, \nu) - \zeta(\gamma))^2 d\gamma \quad (3.11)$$

590 The distribution  $T(\gamma|\hat{\mu}, \hat{\sigma}, \hat{\nu})$  is fit for  
 591 use in generating  $\gamma^*$  random variates at  
 592 a specific  $F^*$  and  $M$ . This approxima-  
 593 tion releases the need to invert  $\zeta$  w.r.t.  $\gamma$   
 594 by using samples of  $\gamma^*$  values to generate  
 595 approximatly uniform samples of  $\zeta(\gamma^*)$ .  
 596 By sampling approximatly uniform  $\zeta(\gamma^*)$   
 597 random variates in this way, and making  
 598 use of the structure in Eq. (3.9), an ap-  
 599 proximate LHS sample can be collected  
 600 via Algorithm (1).

601 For a given  $i$ ,  $\frac{F^*}{M}$  is drawn uniformly  
 602 from within  $\mathcal{F}_i$ . Conditioning on the sam-  
 603 ple of  $F^*$ , and  $M$ ,  $T(\gamma|\hat{\mu}, \hat{\sigma}, \hat{\nu})$  is fit and  
 604  $\gamma^*$  is sampled.  $\zeta^*$  is then computed and  
 605 placed into the appropriate grid element  
 606  $\mathcal{B}_j$ . Given  $\gamma^*$ , the cascade  $\alpha(\gamma^*)$ , and  
 607  $\beta(\alpha(\gamma^*), \gamma^*)$ , can be computed. The al-  
 608 gorithm continues until all of the design elements,  $(\frac{F^*}{M}, \zeta^*) \Leftrightarrow (\alpha^*, \beta^*, \gamma^*)$ , have been  
 609 computed for all  $i \in [1, \dots, n]$ .

---

**Algorithm 1** LHS of size  $n$  on rectangle  $R$ .

---

```

1: procedure  $LHS_n(R)$ 
2:   Define  $n$ -grids  $\mathcal{F}, \mathcal{B} \in R$ 
3:   for each grid element  $i$  do
4:     Draw  $\frac{F^*}{M} \sim Unif(\mathcal{F}_i)$ 
5:     Compute  $[\hat{\mu}, \hat{\sigma}, \hat{\nu}]$  given  $F^*$  &  $M$ 
6:     while  $\mathcal{B}_j$  not sampled do
7:       Draw  $\gamma^* \sim T(\gamma|\hat{\mu}, \hat{\sigma}, \hat{\nu})$ 
8:       Compute  $\zeta^* = \zeta(\gamma^*)$ 
9:       Compute  $j$  such that  $\zeta^* \in$ 
         $\mathcal{B}_j$ 
10:    end while
11:    Compute  $\alpha^* = \alpha(\gamma^*, F^*, M)$ 
12:    Compute  $\beta^* = \beta(\alpha^*, \gamma^*, M, B_0)$ 
13:    Save  $(\frac{F^*}{M}, \zeta^*) \Leftrightarrow (\alpha^*, \beta^*, \gamma^*)$  in  $\mathcal{F}_i \times \mathcal{B}_j$ 
14:  end for
15: end procedure

```

---

#### 610 3.2.4.1 Design Refinement

611 Since the behavior of RP inference, under misspecified models, will vary in yet-  
 612 unknown ways, the exact sampling design density may be hard to know a priori. Sev-  
 613 eral factors, including the particular level of observation uncertainty, high variance (i.e.  
 614 hard to resolve) features of the response surface, or simply "gappy" instantiations of

the initial LHS design may necessitate adaptive design refinement, to accurately describe RP biases. Given the temperamental relationship between RPs and productivity parameters in the Schnute model, a recursive refinement algorithm that makes use of the previously described LHS routine, is developed.

While LHS ensures uniformity in the design margins, and a certain degree of spread, it is widely recognized that particular LHS instantiations may leave substantive gaps in the simulation design. To correct this, LHS is often paired with design elements of maximin design [?, ?]. Maximin designs sample the design space by maximizing the minimum distance between sampled points. This has the advantage of definitionally filling holes in the design, however because no points are ever drawn outside of the design domain, samples tend to clump around edges (particularly corners) of the design domain. Since LHS ensures uniformity in the margins and maximin designs enjoys a certain sense of optimality in how they define and fill gaps [?], the methods are quite complimentary when combined.

Making use of this complimentary relationship, holes in the existing LHS design of RPs are identified based on maximin design principles. New design points are collected based on areas of the RP design space which maximizes the minimum distance between all pairs of points in the current design, based on the following distance function

$$d(\mathbf{x}, \mathbf{x}') = \sqrt{(\mathbf{x} - \mathbf{x}')^T \mathbf{D}^{-1} (\mathbf{x} - \mathbf{x}')} \quad (3.12)$$

$$\mathbf{D} = \mathbf{diag} \left[ \left( \max(\mathcal{F}) - \min(\mathcal{F}) \right)^2, \left( \max(\mathcal{B}) - \min(\mathcal{B}) \right)^2 \right].$$

Above,  $d$  is a scaled distance function that defines the distance between points in the differing scales of  $\frac{B^*}{B_0}$  and  $\frac{F^*}{M}$ .  $\mathbf{D}$  is a diagonal matrix that measures the squared size of the domain in each axis of so as to normalize distances to a common scale.

If  $\mathbf{X}_n$  is the initial design, computed on  $R_{full}$ , let  $\mathbf{x}_a$  be the augmenting point which

maximizes the minimum distance between all of the existing design points,

$$\mathbf{x}_a = \operatorname{argmax}_{\mathbf{x}'} \min\{d(\mathbf{x}_i, \mathbf{x}') : i = 1, \dots, n\}. \quad (3.13)$$

632 The point  $\mathbf{x}_a$  is used as an anchor for augmenting  $\mathbf{X}_n$ . An additional  $LHS_{n'}$  (via  
633 Algorithm (1)) is collected, adding  $n'$  design points, centered around  $\mathbf{x}_a$ , to the overall  
634 design. The augmenting region,  $R_{(\mathbf{x}_a, d_a)}$ , for collecting  $LHS_{n'}$  is defined based on the  
635 square centered at  $\mathbf{x}_a$  with side length  $2d_a$ , where  $d_a = \min\{d(\mathbf{x}_i, \mathbf{x}_a) : i = 1, \dots, n\}$ , in  
636 the space defined by the metric  $d$ .

637 Due to the tendency of maximin sampling to cluster augmenting points on the edges  
638 of the design space,  $R_{(\mathbf{x}_a, d_a)}$  is truncated by the outer most limits of  $R_{full}$  so as to focus  
639 design augmentation within the specified domain of the simulation. Furthermore, since  
640 the design space has a nonlinear constraint at low values of  $\frac{B^*}{B_0}$ , the calculation of  $\mathbf{x}_a$  is  
641 further truncated based on a convex hull defined by the existing samples in the overall  
642 design.

643 Design refinement then proceeds as follows. An initial design is computed,  $\mathbf{X}_n =$   
644  $LHS_n(R_{full})$ , based on an overall simulated region of RPs  $R_{full}$ . The maximin augment-  
645 ing point,  $\mathbf{x}_a$ , is computed at a maximin distance of  $d_a$  from the existing samples. An  
646 augmenting design  $\mathbf{X}_{n'} = LHS_{n'}(R_{(\mathbf{x}_a, d_a)})$  is collected and added to  $\mathbf{X}_n$ . Design refine-  
647 ment carries on recursively collecting augmenting designs in this way until the maximin  
648 distance falls below the desired level.

### 649 3.2.5 refer back to GP?

## 650 3.3 Results

### 651 3.3.1 Design

Algorithm (1) enforces uniform marginals in  $\frac{F^*}{M}$  directly, as well as the adherence of the overall design to latin squares. Figure (3.5) shows a uniform Q-Q plot for sampled  $\zeta$ , using Algorithm (1), against theoretical uniform quantiles. As evidence by the excellent coherence to the theoretical uniform quantiles, the approximation in Section (3.2.4) for sampling  $\gamma$  (and therefore  $\zeta(\gamma)$ ), is very effective. Furthermore since numerical inversion of  $\zeta(\gamma)$  is costly and unreliable, the relative speed and accuracy that this approximate LHS sampling method provides is pivotal for the rest of the work presented here.

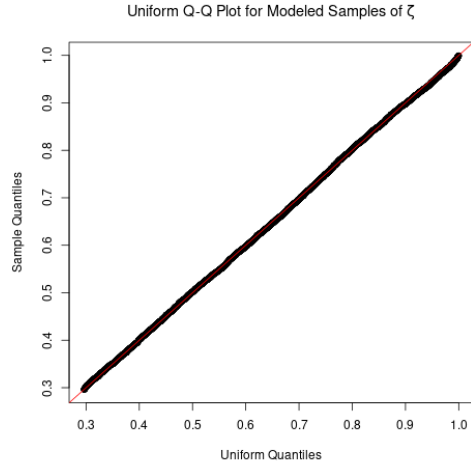


Figure 3.5: Uniform Q-Q plot for  $\zeta$  plotted for  $F^* = 0.1$  and  $M = 0.2$ .

Similarly to the PT model, the three-parameter Schnute model is uniquely identified by each point in the space of  $\frac{F^*}{M}$  and  $\frac{B^*}{B_0}$  RPs. As seen in Figure (3.6), Schnute production has different behaviors in different ranges of RPs space, which are entirely defined by the value of  $\gamma$  (shown in Figure (3.1)). When  $\gamma \geq 1$  the Schnute model produces a family of Logistic-like curves that are increasingly right leaning as  $\gamma$  increases. For  $1 > \gamma \geq 0$ , Schnute production takes a family of left leaning Ricker-like curves that all, at least, approach the x-axis. For  $0 > \gamma > -1$  there are a family of BH-like curves that do not approach the x-axis but still have decreasing productivity for large biomass stocks.

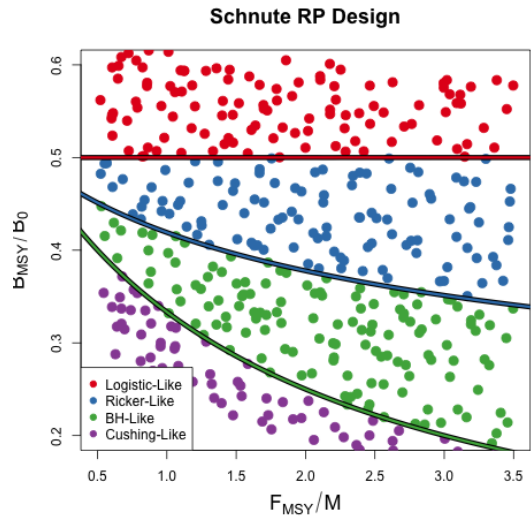


Figure 3.6: A Schnute RP design. Colors indicate different regimes of Schnute production. The black curve shows the BH set.

When  $\gamma$  is exactly  $-1$  Schnute reduces to BH production which has asymptoting production for large biomass. Finally when  $-1 > \gamma$  Schnute produces a family of increasing Cushing-like curves that do not asymptote, and produces linear production as  $\gamma \rightarrow -\infty$ .

Modeling index data that are simulated broadly over the theoretical space of RPs with misspecified BH production greatly limits the range of possible RPs that can be inferred. Under BH production the full theoretical space of RPs are limited to the curve  $\frac{B^*}{B_0} = \frac{1}{F^*/M+2}$ . Define the “BH set” as the set of RPs defined by this limited space, i.e. the curve  $\left\{ \left( \frac{F^*}{M}, \frac{B^*}{B_0} \right) \mid \frac{B^*}{B_0} = \frac{1}{F^*/M+2} \right\}$ . as seen in the **black curve** in Figure (3.6). The farther away from this set that Schnute data are simulated, the more the BH model is misspecified for those data.

### 3.3.2 Metamodeled Trends

Unlike the Schaefer model, the BH set is not a constant in  $\frac{B^*}{B_0}$ . Under the BH model, bias in  $\frac{B^*}{B_0}$  is no longer entirely defined by the degree of model misspecification, but rather the structure of BH RPs allows bias in both  $\frac{B^*}{B_0}$  and  $\frac{F^*}{M}$  to interact as a function of contrast in the data.

#### 3.3.2.1 High Contrast

Figure (3.7) shows metamodeled RP bias surfaces for inference under the BH model in the high contrast setting. The (*left*) and (*bottom*) panels focus only on the  $\frac{B^*}{B(0)}$  and  $\frac{F^*}{M}$  components of bias respectively. In these panels bias is shown as relative bias,  $\frac{\widehat{RP} - RP}{RP}$ , similar to a percent error calculation. Where  $RP$  represents the true value of the three-parameter RP, and  $\widehat{RP}$  refers to the metamodel estimate.

Figure (3.7, *top-right*) combines the components of bias to show the overall map-



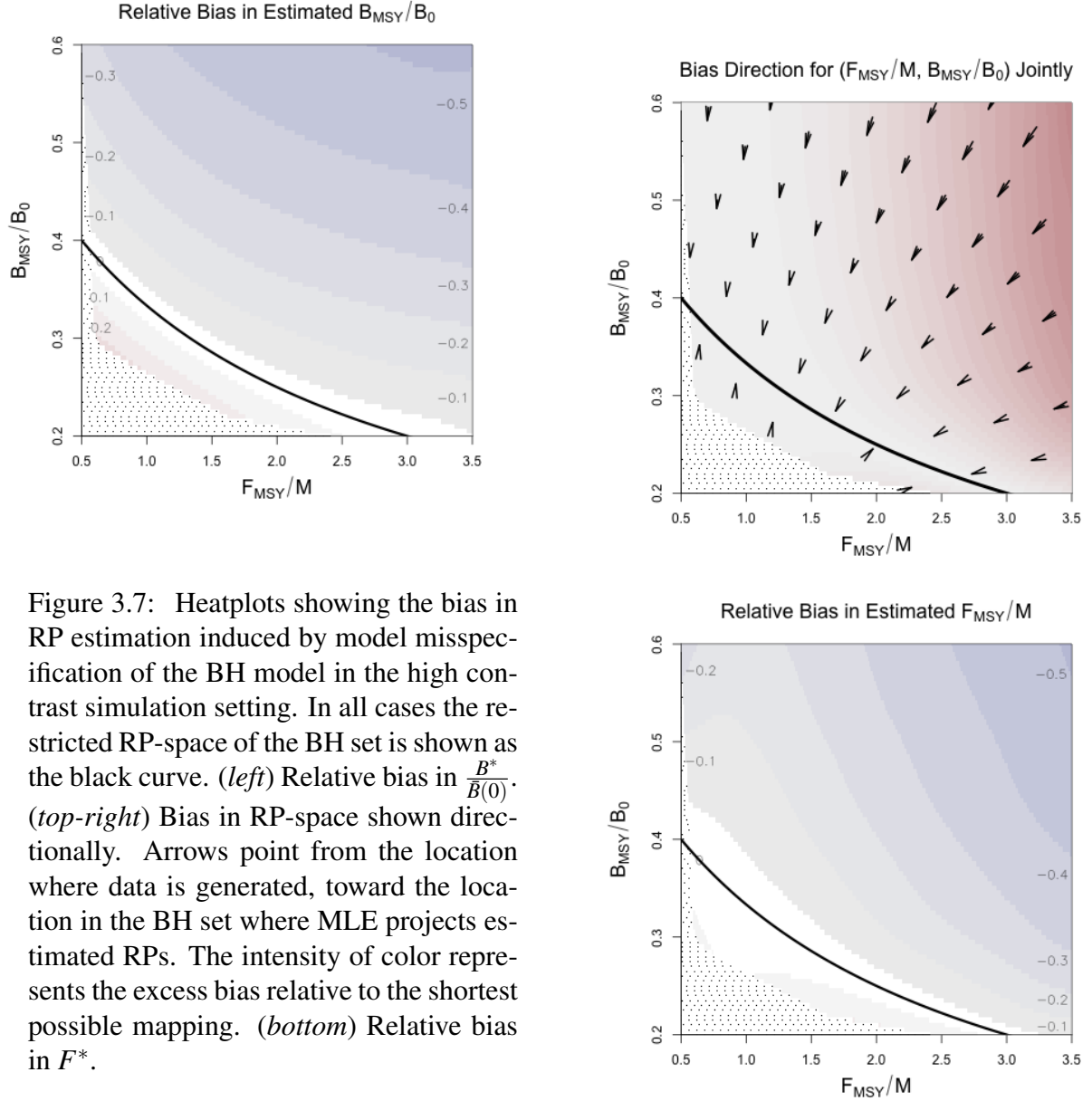


Figure 3.7: Heatplots showing the bias in RP estimation induced by model misspecification of the BH model in the high contrast simulation setting. In all cases the restricted RP-space of the BH set is shown as the black curve. (*left*) Relative bias in  $\frac{B^*}{B(0)}$ . (*top-right*) Bias in RP-space shown directionally. Arrows point from the location where data is generated, toward the location in the BH set where MLE projects estimated RPs. The intensity of color represents the excess bias relative to the shortest possible mapping. (*bottom*) Relative bias in  $F^*$ .

ping of RPs under BH inference in the high contrast simulation setting. Unlike high  
contrast RP inference under the Schaefer model, where mainly bias in  $\frac{B^*}{B(0)}$  occurred, the  
BH model does shows bias in both RPs here. Despite the bias in  $\frac{B^*}{B(0)}$  and  $\frac{F^*}{M}$  these

706 results are similar to that of the Schaefer model in that the overall mapping of RPs is  
 707 very nearly a minimal distance mapping onto the constrained set of RPs. The primary  
 708 difference between Schaefer model and BH RP inference is the geometry of their lim-  
 709 ited RP spaces. Unlike the Schaefer model the BH set encourages bias in both RPs for  
 710 misspecified models even in very well informed setting.

### 711 3.3.2.2 Low Contrast

712 Figure (3.8) shows the mapping of  
 713 RPs in the low contrast simulation set-  
 714 ting. Figures (3.8) and (3.7, *top-right*)  
 715 share a common scale for the intensity  
 716 of color to facilitate comparison. In Fig-  
 717 ure (3.8) notice that the mildly misspec-  
 718 ified area around the BH set produces  
 719 mappings onto the BH set which resem-  
 720 ble the minimal distance mapping seen  
 721 in the high contrast setting. The primary  
 722 difference in this low contrast setting, is  
 723 the break point around  $\frac{B^*}{B(0)} = 0.4$  above  
 724 which  $\frac{F^*}{M}$  is sharply underestimated.

725 The region of RPs where the BH  
 726 model manages to recover the minimal  
 727 distance mapping may be considered a “safe regime” of data types that are reason-  
 728 ably well modeled by a BH model. By comparison of Figure (3.8), with Figure (3.6),  
 729 this safe regime of the BH model occurs for data generated for Cushing-like or BH-like  
 730 production. While bias of the RPs can still become concerningly large, this region can  
 731 be considered safe in the sense that even for low contrast data RP estimation under the

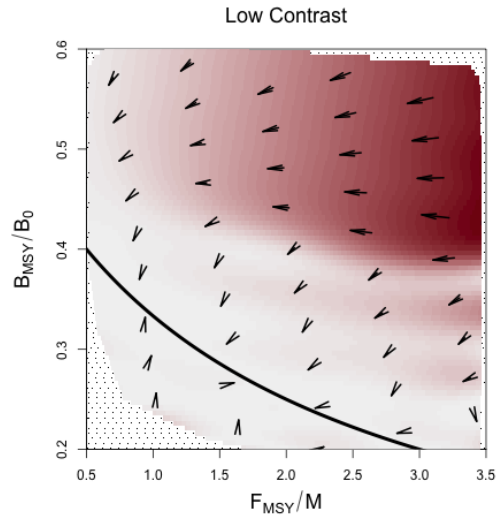


Figure 3.8: Joint bias direction of RP inference in the low contrast simulation setting. The intensity of color represents the excess bias relative to the shortest possible mapping.

the BH model recovers the minimal distance mapping.

Outside of this safe regime, RP estimation breaks from the minimal distance mapping at the interface between BH-Like and Ricker-Like regimes of the Schnute model (again see Figure (3.6)). The Ricker model lies along this regime interface, and represents the first model to approach the x-axis for large biomasses as  $\gamma$  increases. This markedly unBH-like productivity in the low information simulation setting breaks MLE inference from the minimal distance mapping and

instead maps RPs to extremely low values of  $F^*$ ; consequently  $\frac{B^*}{\bar{B}(0)}$  is estimated near the limiting value under the BH (i.e.  $\lim_{F^* \rightarrow 0} \frac{1}{F^*/M+2} = 0.5$ ). Similarly the set of Ricker RPs (as well as the Schaeffer set) include this trivial limiting point in common ( $\frac{F^*}{M} = 0$ ,  $\frac{B^*}{\bar{B}(0)} = 0.5$ ).

Interestingly, in the high contrast setting this trivial mapping for highly misspecified BH models is not present. This suggests that, under a misspecified BH model, the presence of adequate information in the data to produce reasonable estimates of  $\frac{F^*}{M}$ , drives  $\frac{B^*}{\bar{B}(0)}$  below 0.5 in accordance with  $\frac{B^*}{\bar{B}(0)} = \frac{1}{F^*/M+2}$ , even when the true  $\frac{B^*}{\bar{B}(0)} > 0.5$ . This phenomena balances RP estimation within the constrained BH set as mediated by the information content of the data and the degree of model misspecification. When the information content in the data is too small to drive a compromised RP estimate, inference completely disregards accurate estimation of  $F^*$  in order to better estimate  $\frac{B^*}{\bar{B}(0)}$  by exploiting the common limiting behavior of the BH set and that of Ricker-like and Logistic-like models.

Estimated Yield Curves For Poorly Specified BH

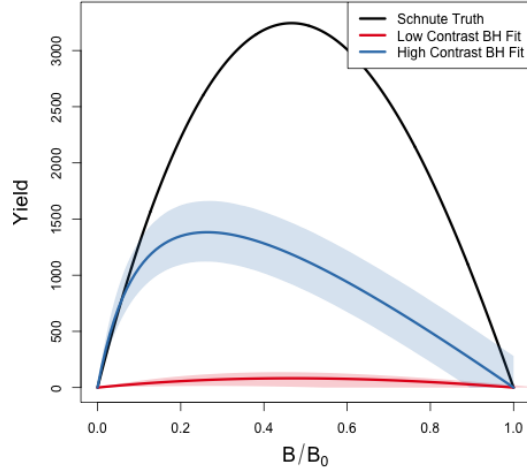


Figure 3.9: Yield curves for data generated with  $\frac{F^*}{M} = 3.48$  and  $\frac{B^*}{\bar{B}(0)} = 0.48$ .



## 3.4 Discussion

### *Tease Out BH*

Results presented here generally agree with what is known about estimating population growth rate parameters [?, ?, ?]. These studies appreciate the role of contrast for estimating growth rates, however they struggle to make generally extensible conclusions since they focus only on a handful of stocks that fall short of forming a random sample of the greater population of possible stock behaviors. The LHS design methods presented here are designed specifically to simulate a representative sample of stocks broadly across the space of possible RPs. Furthermore, the simulation design, taken together with the GP metamodel of productivity parameter estimates, allows this study to control the degree of model misspecification and generalize conclusions about the behavior of productivity estimation within the production model setting presented.

In the presence of contrast,  $F^*$  estimation can enjoy very low bias even for a wide range of poorly specified models; conversely in the absence of contrast  $F^*$  estimation can suffer very large bias even for slightly misspecified models. This pattern is particularly true for low-contrast inference under the Schaefer model where the geometry of the restricted RP set isolates estimation failure of  $F^*$  from  $\frac{B^*}{\bar{B}(0)}$ . While contrast has a similar impact on  $F^*$  estimation under the BH model, the geometry of the BH RP set correlates estimation bias of  $F^*$  and  $\frac{B^*}{\bar{B}(0)}$ . The GP metamodeling approach reveals a more general pattern that highly informative data sets (high contrast) produces a nearly minimal distance mapping of RPs onto the constrained RP set.

In all cases when model misspecification is removed, even with weakly informative data, RP estimation is unbiased and well estimated. Thus contrast alone is not the only factor leading to inferential failure. Model misspecification is a necessary but not sufficient condition for inducing RP estimation bias. The particular RP bias present

depends on the RP geometry of the fitted model and how that geometry is misspecified relative to the data. The RP mapping is then oriented to the RP geometry of the fitted model.

While the relative fishing rate parameterized in Section (2.2.6) captures a usefully broad spectrum of relevant fishing behaviors, it is still limiting in the amount of information that it can induce. Improved methods for quantifying contrast in fisheries data, and/or methods for discovering more informative fishing behavior, could improve this analysis. In the absence of maximally informative dataset simulation methods will not fully describe how inference fails, but the methods presented here tell the most complete picture yet, with explicit control of the degree model misspecification, contrast, and a simulation design that allows for uniform representative data generation across biologically meaningful stocks. The results presented here suggest the conjecture that under a maximally informative dataset, RP inference with a two parameter production function will be biased in the direction a shortest distance map from the true RPs onto restricted set of RPs under the two-parameter model.

Given the potential for model misspecification of RPs, a minimal distance mapping of RPs represents a best-case scenario where the total bias of RPs, when measured jointly, is minimized. That said, without recognizing the geometry of how two-parameter models of productivity limit RP space this may lead to unintuitive implications in RP estimation. For example, due to the shape of the BH RP set a minimal distance mapping ensures that if there is bias in one of  $\frac{B^*}{B_0}$  or  $F^*$ , there will necessarily be bias in the other RP. However under the Schaefer model, since the RP set is a constant in  $\frac{B^*}{B_0}$ , bias in  $F^*$  is not adulterated in the same way by bias in  $\frac{B^*}{B_0}$  estimation. While models with constant RPs, such as the logistic model  $\frac{B^*}{B_0} = \frac{1}{2}$  or the Fox model  $\frac{B^*}{B_0} = \frac{1}{e}$ , are extremely limited, they can be valuable tools for developing intuition precisely because they isolate RP estimation in their free RPs from the correlated RP biases present in models like the BH or Ricker model.

813 When one considers the implications of RP bias, overestimation of RPs carries the  
814 severe implication of management recommendations potentially leading to overfishing,  
815 while underestimation of RP leads to overly conservative management. In this sense,  
816 when the true model is not known, the geometry of the BH set together with the meta-  
817 modeled bias trends makes the BH model a naturally conservative estimator of RPs for  
818 most stocks. For most non-BH populations the BH model is likely to make conservative  
819 errors in its estimates of  $F^*$  and  $\frac{B^*}{B_0}$ . The one notable exception to the conservatism of  
820 the BH model stands for data generated in the Cushing-like regime of Schnute RPs. In  
821 this regime the BH model tends to be fairly unbiased overall, however the bias that is  
822 present for these populations tends to be overestimation in both RPs, leading to much  
823 more severe management consequences for those populations.

824 The RP bias trends of the Schaefer model demonstrate much less conservatism than  
825 For any population with  $\frac{B^*}{B_0} < 0.5$ ,  $\frac{B^*}{B_0}$  will be overestimated. When the population  
826 comes from the regime where  $\frac{B^*}{B_0} > 0.5$ ,  $\frac{B^*}{B_0}$  will be under estimated, but  $F^*$  is likely  
827 to be overestimated depending on the degree of contrast present in the data. So while  
828 the Schaefer model is an intuitive model, it tends to lead to much less conservative RP  
829 estimation.

830 While it is important to recognize these limitations of two-parameter models of  
831 productivity, we should not solely accept conservatism as a rationale of choosing a  
832 BH model of productivity. Increasing the flexibility of the production function by  
833 moving toward three-parameter models would release the underlying structural limi-  
834 tations [?] that cause these RP biases in the first place. Punt & Cope [?] considers a  
835 suite of possible three-parameter curves which could be used instead of current two-  
836 parameter curves. For all of their benefits, three parameter production functions have  
837 their own complicating factors, and the structure present in the Schnute model explored  
838 here makes it an intuitive bridge model for developing three-parameter models going  
839 forward.

## 840 **Chapter 4**

### 841 **A Delay Differential Model**



## 4.1 Introduction

While the SPM captures the majority of variation in RPs, individual growth is the next most influential dynamic for explaining RP variation [cite or generalize](#). The SPM captures the net effect of biomass production by modeling all aspects of biomass production (i.e. maturity, recruitment, growth, etc.) together in the production function. While there are a number of approaches to modeling these dynamics [cite age structured model, selectivity models, any other model I can find \(Munch, Bethany?\)](#), in current best practice for management age structured models (ASM) are used when the data are available [cite SS3, or new thing](#). However ASM require a lot of expensive data to fit; furthermore even when the data do exist, the highly parameterized structures used to model these data introduce the potential for identifiability issues [cite](#).

An intermediate approach between SPM and ASM is the delay differential model (DDM). Simple DDM models do not necessarily model individual growth [cite EJ Alec and Aalto et al. 2015](#), but even so the delayed structure of the model is beneficial in modeling the lag from egg to recruitment as well as the natural autocorrelation often observed with stock size. Some DDMs explicitly tease out the dynamics of individual growth and maturity from recruitment to explain net production as separate but interconnected processes [cite schnute, deriso \[?\], \[?, pg. 334\], Quinn and Deriso 1999](#)

✓ SPM describe productivity via net recruitment of biomass, natural mortality and fishing.

- ASM describe recruitment in numbers, individual growth to biomass, natural mortality, fishing, and selectivity.
- selectivity requires a lot of data to parameterize and describe.
- in a data poor setting, DDM offer an effective intermediate.
- RPs are largely determined by R, and to a much lesser effect growth.

- 867 • growth is often estimated external to the dynamics model, although we will see
- 868 that in certain situations an index can inform growth as well.
- 869 •
- 870 • intermediate in complexity between SPMs and ASMs. (Next step in complexity)
- 871 • perfect size model for data poor stocks, when some knowledge about growth may
- 872 be known but not the full age at length table of an age structured model [?]
- 873 • These models include natural mortality, and may or may not [?] incorporate in-
- 874 dividual (somatic) growth.
- 875 •
- 876 • time series fisheries data (catch, biomass and/or numbers)
- 877 • delay structure naturally represents time from egg to recruitment, and the natural
- 878 auto correlation of stock size with itself.
- 879 • natural mortality
- 880 •
- 881 • RP calculation have been elusive [?, ?].
  - 882 – [?] gives results for BH, Ricker, and three parameter Shepard
  - 883 – I give results for Schnute which includes BH, Ricker, Schafer, and Cushing
  - 884 as a a special case.
- 885 • data poor setting
- 886 • fitted to time series of fishery data
- 887 • received little attention in developing MSY-based RPs or proxies 2015, 2022

- 888 • intermediate in complexity between SPMs and ASMs.
- 889 • allows development of RPs. The unanimous answer was: “No;
- 890 • MSY-based RPs (e.g., Aalto et al. 2015),
- 891 • Relates:
  - 892 – lag: (i) to the number of years from egg deposition until the young fish
  - 893 become vulnerable to the fishery,
  - 894 –  $B_{t-lag}$ : (ii) to the fact that the exploitable stock size in any time step depends
  - 895 on stock sizes in previous time steps,
- 896 • These models include natural mortality, individual growth
- 897 • that the populations’ recruit
- 898 • adult components can be tuned by separate indices of abundance in number,
- 899 weight, or both.
- 900 • (i) constant growth and mortality rates
- 901 • (ii) equal ages of knife-edge selectivity (i.e., recruitment to the fishery) and knife-
- 902 edge maturity, implying that adults and recruits in the population are fully se-
- 903 lected and have equal (full) reproductive capacity.
- 904 • Management of “data-rich” stocks is often based on complex assessments that in-
- 905 corporate a variety of data sources and that provide estimates of stock status, vari-
- 906 ous management targets or reference points, and sustainable yield. There remain
- 907 very many fish stocks for which data are too limited to support these data-rich
- 908 approaches. The focus of assessment for “data-poor” stocks is often restricted
- 909 to estimates of sustainable yield because insufficient data are available to esti-
- 910 mate the full suite of reference points. Common approaches for data-poor stocks

911 include defining a proxy value for sustainable catch ( $F_{msy}$  proxy), e.g. recent  
912 average catch, which may be precautionarily reduced to account for uncertainty.  
913 Advice regarding the extent of these reductions has been based on qualitative de-  
914 scriptions of stock status, such as “above Bmsy” or “overfished” (Restrepo et al.,  
915 1998).

- 916 • data poor model with lots of flexibility and RPs
- 917 • no individual growth
- 918 • the delay model: [?] [?] [?].
- 919 • discrete: [?, pg. 334], Quinn and Deriso 1999
- 920 • [?] cDDM model
- 921 • automatic accounting for cohort cycles
- 922 • Huynh 2020
- 923 • Licanideo et al. 2023 cDDM MSE
- 924 • Munyandorero 2012, 2015, 2022, 2023\*
- 925 • Shertzer and Conn (2012), the BH–SRR should be the default choice in analyses  
926 unless there are mechanisms, such as cannibalism or depletion of food resources,  
927 that favor the R–SRR or the S–SRR].
- 928 • ignorance of how generate RPs with DD models [?].

## 929 **4.2 Methods**

### 930 **4.2.1 Delay Differential Model**

Age structured fisheries models typically assume [?, VB] growth in length with age. To model weight the assumption of VB growth in length is composed with a power law relating length to weight,  $w = al^b$ . Since  $b$  is usually  $\sim 3$  this composition of assumed functional forms typically results in a monotonically increasing sigmoidal curve of weight with age. When  $b \leq 1$  weight at age takes a VB-like form with  $b = 1$  resulting in an exact correspondence of simultaneous VB-growth in length and weight.

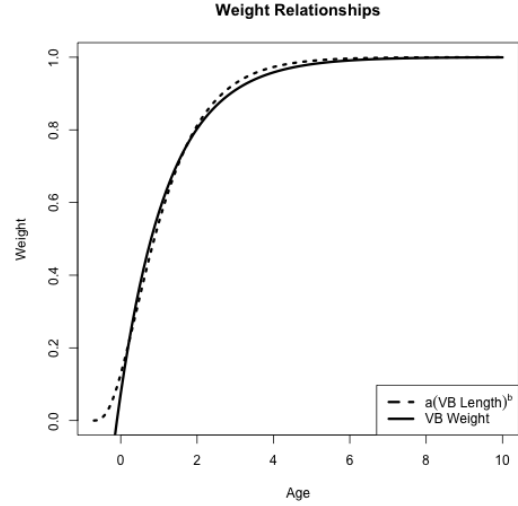


Figure 4.1: The typical composition of allometric weight ( $b = 3$ ) with VB growth in length, as approximated by VB growth in weight directly.

The delay model slightly abridges these relationships by directly assuming VB growth in weight as follows,

$$w(a) = w_{\infty}(1 - e^{-\kappa(a-a_0)}). \quad (4.1)$$

$\kappa$  is a parameter that controls the instantaneous rate of individual growth (in weight) with age.  $w_{\infty}$  is the maximum weight of individuals in the population, and  $w(a)$  is the average weight of an individual at age  $a$ . The parameter  $a_0$  controls the age at which individuals are assumed to have zero weight; by letting  $a_0 < 0$  this allows fish of age zero to have positive weight. Rather than taking a sigmoidally increasing function, VB growth directly in weight results in a monotonically increasing curve that asymptotes with a strictly decreasing growth rate with age. (only a good approximation for older ages where growth begins to decline)

Together with VB growth, the delay model is derived from the assumption that both natural mortality and fishing selectivity are separately proportional to a common

953 heavyside step function with age. That is to say, before a threshold age of selectivity,  
 954  $a_s$ , the population is assumed not to experience any mortality whatsoever, but all fish  
 955 older than  $a_s$  experience the same rate of natural mortality. Simultaneously all fish older  
 956 than  $a_s$  are equally vulnerable to fishing (i.e. knife edge selectivity at age  $a_s$ ), although  
 957 fishing effort may vary from through time.

[?] shows that within these assumptions the following delay differential system of equations exactly models the population dynamics of the total exploitable biomass  $B(t)$  and number of individuals  $N(t)$  through time.

$$\frac{dB}{dt} = w(a_s)R(B; \theta) + \kappa[w_\infty N - B] - (M + F)B \quad (4.2)$$

$$\frac{dN}{dt} = R(B; \theta) - (M + F)N \quad (4.3)$$

958 This formulation separates the number of individuals in the population from the  
 959 biomass of the population. The dynamics of  $N$ , as seen in Eq (??), are very similar to  
 960 that of the **production models previously presented**, however the role of the production  
 961 function is now filled by a "recruitment" function,  $R(B)$ , which describes the number  
 962 of new individuals recruiting into the exploitable population as a function of exploitable  
 963 biomass. In turn, the biomass dynamics are coupled to the numbers dynamics by the  
 964 assumption of VB growth with growth parameters appearing in Eq (??), converting  
 965 population numbers into biomass and accounting for the growth of biomass with age.

966 Eq (??) of the above model expands the notion of biomass production into the pro-  
 967 cesses of recruitment, individual growth, and maturity. The term  $w(a_s)R(B; \theta)$  repre-  
 968 sents the biomass of new recruits; with  $w(a_s)$  representing the weight of individuals at  
 969 the age of maturity,  $a_s$ , and  $R(B; \theta)$  representing the number of new recruits entering the  
 970 exploitable population at time  $t$ . The negative term,  $(M + F)B$ , represents all causes of  
 971 mortality as it is applied to biomass. Finally, the term  $\kappa[w_\infty N - B]$  accounts for the net  
 972 growth of the existing biomass by discounting the limiting maximal individual growth

973 rate by metabolic weight loss proportional to  $B(t)$ . This term, together with the delay  
 974 structure in  $R$ , provides the major computational savings of the delay differential set-  
 975 ting, as compared with full age structured models, by automatically keeping track of  
 976 changes in the mean size and growth associated with changes in recruitment as cohorts  
 977 mature into the population.

Often a BH functional form is assumed for the stock recruitment relationship, but  
 any adequately flexible family of functions may model this relationship. For the sake  
 of evaluating the adequacy of assumed BH recruitment the simulation setting below is  
 derived for the delay model under the assumption of the generalized three parameter  
 Schnute recruitment as follows.

$$R(B; [\alpha, \beta, \gamma]') = \alpha B(t - a_s)(1 - \beta \gamma B(t - a_s))^{\frac{1}{\gamma}} \quad (4.4)$$

978 The parameters  $\theta' = [\alpha, \beta, \gamma]$  function similarly in this setting as previously described  
 979 in Section (??). That said, since the delay model explicitly parses out growth in it's  
 980 dynamics, these parameters only describe the net processes of larval production, and  
 981 maturation into the population, where as the production model used these parameters to  
 982 also model the net effects of growth on biomass production. The  $\gamma$  parameter general-  
 983 izes the family to model varying degrees of decreasing recruitment for large biomasses  
 984 as  $\gamma$  increases. The Schnute function is exactly equivalent to BH recruitment at the  
 985 special case when  $\gamma = -1$ , it passes through the Ricker model as  $\gamma \rightarrow 0$ , and Logistic  
 986 recruitment occurs when  $\gamma = 1$ .

987 Since the delay model assumes knife edge selectivity, at age  $a_s$ , the term  $B(t -$   
 988  $a_s)$  appears in  $R$ . That is to say fish recruiting into the exploitable population are the  
 989 result of larval production of biomass  $a_s$  time units in the past. This is because fishing  
 990 selectivity is only assumed to occur for fish that are at least  $a_s$  time units old and thus  
 991 fish younger than  $a_s$  are not exploitable. This waiting period requires that new recruits

992 be the result of spawning biomass  $a_s$  time units in the past. Modeling maturity in this  
 993 way results in dynamics equations which are a system of delay differential equations as  
 994 opposed to the simple ODEs that arise in the production model setting.

995  $\sim$  interpretation of recruitment (larval production, recruitment) [growth external]  
 996 vs. production (larval production, recruitment, growth)

997 • general structure: [?] [?, pg. 334]

998 • growth: [?]

999 • recruitment: [?, ?]

## 1000 4.2.2 Reference Points

1001 Deriving reference points for the delay model under Schnute recruitment is con-  
 1002 ceptually similar to the production model setting. The additional nonlinear VB growth  
 1003 assumptions along side Schnute recruitment quickly make the expressions look some-  
 1004 what unweildy, although analytical solutions can still be derived for most of the same  
 1005 quantities (although complicated by growth parameters).

Starting from Eqs. (??) and (??), setting both  $\frac{dB}{dt}$  and  $\frac{dN}{dt}$  simultaneously equal to zero, and solving for  $B$  and  $N$  as a function of fishing, gives the equilibrium biomass and numbers equations.

$$\bar{B}(F) = \frac{1}{\beta\gamma} \left( 1 - \left( \frac{(F+M)(F+M+\kappa)}{\alpha w(a_s)(F+M + \frac{\kappa w_\infty}{w(a_s)})} \right)^\gamma \right) \quad (4.5)$$

$$\bar{N}(F) = \frac{\alpha \bar{B}(F)(1 - \beta\gamma \bar{B}(F))^{1/\gamma}}{F+M} \quad (4.6)$$

1006 Eq. (??) is just  $\frac{R(\bar{B})}{F+M}$ , and is coupled to  $\bar{B}(F)$  where most of the dynamics appear. Eq.  
 1007 (??) resembles Eq (3.3) from the simple production model setting although the growth



parameters  $\kappa$ ,  $w_\infty$  and  $w(a_s)$ , make slight adjustments to the balance of the maximum rate of recruitment and mortality rate to give an expression for equilibrium biomass that accounts for the factors of individual growth.

Expressions for  $B_0$  and  $B^*$  are attained by evaluating  $\bar{B}(F)$  at  $F = 0$  and  $F = F^*$  respectively. Calculation of  $F^*$  typically involves maximization of equilibrium yield,  $\bar{Y} = F\bar{B}(F)$ . While it was not possible to analytically maximize  $\bar{Y}$ , stable numerical solutions for calculating  $F^*$  were obtained by numerically solving for the roots of the analytical derivative of equilibrium yield with respect to  $F$ . Below a greatly simplified expression for  $\frac{d\bar{Y}}{dF}$  is shown; the substitution  $Z = F + M$  (total mortality rate) has been made to produce a more compact expression.

$$\frac{d\bar{Y}}{dF} = \frac{1}{\beta\gamma} \left[ 1 - \left( \frac{Z(Z+\kappa)}{\alpha w(a_s)(Z + \frac{\kappa w_\infty}{w(a_s)})} \right)^\gamma - \left( \frac{\gamma F}{\alpha w(a_s)} \right) \left( \frac{Z(Z+\kappa)}{\alpha w(a_s)(Z + \frac{\kappa w_\infty}{w(a_s)})} \right)^{\gamma-1} \left( 1 + \frac{\left( \frac{\kappa w_\infty}{w(a_s)} \right) \left( \kappa - \frac{\kappa w_\infty}{w(a_s)} \right)}{\left( Z + \frac{\kappa w_\infty}{w(a_s)} \right)^2} \right) \right] \quad (4.7)$$

$F^*$  is calculated as the numerical root, w.r.t.  $F$ , of the above expression. The numerical root is calculated using the base R uniroot function which employs a derivative free search given by [?].

#### 4.2.2.1 BH Constraint

In the simple production model the BH constrained RPs are fixed to  $\frac{1}{x+2}$ . In the delay differential modeling setting the constrained BH RP set is complicated by the growth parameters  $a_s$  and  $\kappa$ . Under BH recruitment these parameters of the delay model slightly influence this relationship as seen in Figure (??). That said, the influence of  $a_s$  and  $\kappa$  on RPs is still largely limited to a confined region of ref-

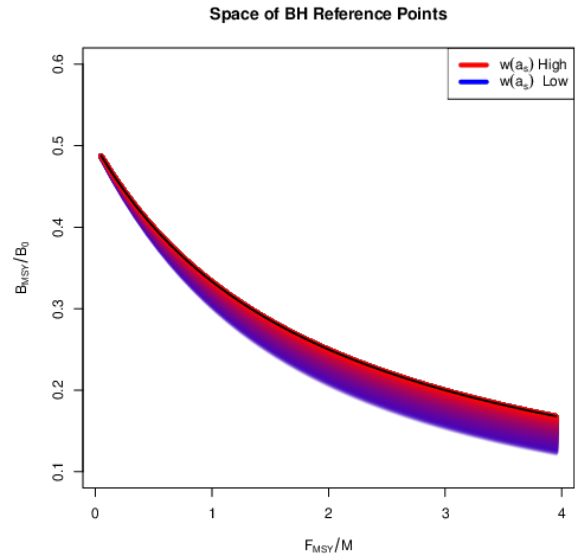


Figure 4.2: The space of BH RPs for the delay model as a function of  $\kappa$  and  $a_s$ . The RP space is plotted for  $80 \times 80$  combinations of  $\kappa \in [0.1, 2]$  and  $a_s \in [0.1, 10]$ . The color drawn is the resulting value of  $w(a_s)$  mapped between blue and red.  $\frac{1}{x+2}$  is plotted in black for reference.

1032 erence point space which resembles the  
 1033  $\frac{1}{x+2}$  form. In fact the confined region of  
 1034 RPs is bounded above by  $\frac{1}{x+2}$ . In Figure  
 1035 (??) notice that for values of  $a_s$  and  $\kappa$  that result in high  $w(a_s)$  (high values of  $\kappa$  and  
 1036 small values of  $a_s$  seen in red) the BH RP space converges to  $\frac{1}{x+2}$  as derived in the  
 1037 simple production model setting. In opposition to the simple production model limit,  
 1038 when  $w(a_s)$  is low (as seen in the more blue region of Figure(??)), RPs decrease as the  
 1039 influence of growth in the dynamics increases.

### 1040 4.2.3 Delay Differential Integration

1041 The delay model belongs to a class of differential equations known as delay dif-  
 1042 ferential equations (DDE). The delay arises from the  $B(t - a_s)$  terms found in the  
 1043 recruitment function. Solving DDEs require special care which depends on the nature  
 1044 of the time delay. The addition of time-varying delays, many different delays, or very  
 1045 small delays (delays below the step size of the numerical integrator) results in some  
 1046 of the more challenging settings for solving DDEs. However with a single stationary  
 1047 model of the age of selectivity, the delay model in this setting represents one of the most  
 1048 straight forward DDE structures. The most numerically challenging case presented here  
 1049 arises in the case of the limiting production model when  $a_s \rightarrow 0$  while  $\kappa \rightarrow \infty$ . That  
 1050 said the limiting production model can be approximated for values of  $a_s \approx 0.1$ , and it  
 1051 was straightforward to ensure that the step size of the integrator remained reasonably  
 1052 below 0.1.

1053 The DDE presented here is integrated with the initial values fixed at  $B_0$  and  $N_0$  as  
 1054 given by Eqs. (??) and (??) with  $F = 0$  at any given configuration of  $\theta$  and growth pa-  
 1055 rameters. The system given in Eqs. (??) and (??) are then solved numerically using the  
 1056 implicit Livermore Solver (lsode) as implemented in the `dede` function of the R pack-  
 1057 age `deSolve` [?]. The `dede` solver provides many methods for integrating DDEs, but

1058 Isode was chosen because it is an implicit method that runs relatively quickly with a rel-  
 1059 atively smaller footprint in system memory as compared with other methods. The radau  
 1060 method was also tried in more computationally challenging settings with good results  
 1061 (albeit running more slowly than Isode). Ultimately the simulated parameter space did  
 1062 not produce DDEs that require the more expensive radau integrator to solve accurately.

#### 1063 4.2.4 Simulation Design

1064 Similarly as previously described in Section (3.2.2) the relationship between RPs  
 1065  $\mapsto \theta$  cannot be fully expressed analytically for the Schnute delay model. However,  
 1066 just as in the production model setting, simulation only requires enough knowledge of  
 1067 these mappings to gather a list of  $(\alpha, \beta, \gamma)$  tuples and the corresponding RPs in some  
 1068 reasonable space-filling design over RP space.

1069 In the delay model a partial mapping for  $(F^*, B_0) \mapsto (\alpha(\cdot, \gamma), \beta(\cdot, \cdot, \gamma))$  can be de-  
 1070 rived analytically in terms of RPs and  $\gamma$ . The substitution  $Z^* = F^* + M$  is made where  
 1071  $F^*$  and  $M$  appear together to produce a more compact expression.

$$\alpha = \left[ \left( \frac{Z^*(Z^* + \kappa)}{w(a_s)(Z^* + \frac{\kappa w_{\infty}}{w(a_s)})} \right)^{\gamma} + \left( \frac{\gamma F^*}{w(a_s)} \right) \left( \frac{Z^*(Z^* + \kappa)}{w(a_s)(Z^* + \frac{\kappa w_{\infty}}{w(a_s)})} \right)^{\gamma-1} \left( 1 + \frac{\left( \frac{\kappa w_{\infty}}{w(a_s)} \right) \left( \kappa - \frac{\kappa w_{\infty}}{w(a_s)} \right)}{(Z^* + \frac{\kappa w_{\infty}}{w(a_s)})^2} \right) \right]^{\frac{1}{\gamma}} \quad (4.8)$$

$$\beta = \frac{1}{\gamma B_0} \left( 1 - \left( \frac{M(M + \kappa)}{\alpha w(a_s)(M + \frac{\kappa w_{\infty}}{w(a_s)})} \right)^{\gamma} \right) \quad (4.9)$$

Above Eq. (??) results from setting Eq. (3.7) equal to zero and solving for  $\alpha$ , and  
 Eq. (??) results from solving the  $\bar{B}(0)$  expression, as derived from Eq. (??), for  $\beta$ . The  
 system is completed by further working with the  $\frac{\bar{B}(F^*)}{\bar{B}(0)}$  expression, as seen below, to

identify  $\gamma$ .

$$\frac{B^*}{B_0} = \frac{1 - \left( \frac{(F^*+M)(F^*+M+\kappa)}{\alpha w(a_s)(F^*+M+\frac{\kappa w_\infty}{w(a_s)})} \right)^\gamma}{1 - \left( \frac{M(M+\kappa)}{\alpha w(a_s)(M+\frac{\kappa w_\infty}{w(a_s)})} \right)^\gamma} \quad (4.10)$$

1072 The system formed by collecting Eqs. (??), (??), and (??) can be navigated simi-  
 1073 larly to Eq. (3.9) in the Schnute production model setting. For a population experienc-  
 1074 ing natural mortality  $M$ , VB growth with paramters  $\kappa$  and  $w_\infty$ , and age of selectivity  $a_s$   
 1075 the above system can fully specify  $\alpha$  and  $\beta$  for a given  $\gamma$ , by fixing  $F^*$ ,  $B_0$ , and  $\frac{B^*}{B_0}$ . For a  
 1076 given  $\gamma$  a cascade of closed form solutions for  $\alpha$  and  $\beta$  can be obtained, just as in Section  
 1077 (3.2.2). First  $\alpha(\gamma)$  can be computed, and then  $\beta(\alpha(\gamma), \gamma)$  can be computed. If  $\alpha(\gamma)$  is  
 1078 filled back into the expression for  $\frac{B^*}{B_0}$ , the system collapses into a single onerous expres-  
 1079 sion for  $\frac{B^*}{B_0}(\alpha(\gamma), \gamma)$ . For brevity, define the function  $\zeta(\gamma) = \frac{B^*}{B_0}(\alpha(\gamma), \gamma, F^*, M)$  based on  
 1080 Eq. (??).

1081 Again rather than inverting  $\zeta(\gamma)$  for  $\gamma$ ,  $\gamma$  is the sampled so that the overall simulation  
 1082 design is space filling as described in Section (3.2.4). Given the sampled  $\gamma$ , the cascade  
 1083 of  $\alpha(\gamma)$ , and then  $\beta(\alpha(\gamma), \gamma)$ , can be computed, and the Schnute delay model is fully  
 1084 defined by a given  $(\frac{F^*}{M}, \frac{B^*}{B_0})$ . While conceputally this framing is similar to the Schnute  
 1085 production model, the analytical expressions are more complex, and numerically trech-  
 1086 erous, since growth parameters appear explicitly here. Other ways of navigating the  
 1087 RPs  $\mapsto \theta$  system are possible, but for the sake of numerical stability this strategy has  
 1088 proven the most reliably accurate by limiting exposure to numerical error propogation.

1089 Each design location defines a complete Schnute delay differential model with the  
 1090 given RP values. Indices of abundance are simulated from the Schnute model at each  
 1091 design location, a small amount of residual variation,  $\sigma = 0.01$ , is added to the simu-  
 1092 lated index, and the data are then fit with a misspecified BH model. The design captures  
 1093 various degrees of model misspecification relative to the BH model, so as to observe

1094 the effect of recruitment misspecification upon RP inference.

1095 point to catch, and LHS design, and Metamodel.

## 1096 4.2.5 Parameter Estimation

1097 • I use B only here

1098 • quick statement of inference, and reference to previous section

Let  $I_t$ ,  $t \in \{1, 2, 3, \dots, T\}$ , be a series of indices of abundance, proportional to biomass, as simulated from the Schnute Delay model. These data are modelled with the following log-normal observation model that has been intentionally constrained to BH recruitment,

$$I_t \sim LN(qB_t(\theta, \phi), \sigma^2). \quad (4.11)$$

1099  $B_t(\theta, \phi)$  is the biomass solution of the BH constrained DDE system. The BH constraint  
1100 is implemented by fixing  $\gamma = -1$  so that  $\theta' = [\alpha, \beta, \gamma = -1]$ .  $\phi$  is a vector of growth  
1101 and maturity parameters,  $\phi' = [\kappa, w_\infty, a_0, a_s]$ . The nuisance parameter  $q$  models the  
1102 proportionality constant of the index with process biomass, and  $\sigma^2$  models residual  
1103 variation of the index.

1104 In this setting,  $\phi$  and  $q$  are fixed to focus on the inferential affects of model misspec-  
1105 ification on recruitment parameters and RPs. Without an explicit mechanism for the  
1106 delay model to incorporate age data, under the BH model  $\phi$  is not well informed and  
1107 would typically be estimated externally for data limited stocks. Under BH recruitment  $\phi$   
1108 can only slightly impact RPs as seen in Figure (??).

1109  $\sigma^2$  and  $\theta$  are reparameterized to the log scale and fit via MLE. Reparameterizing  
1110 the parameters to the log scale improves the reliability of optimization, in addition to  
1111 facilitating the use of Hessian information for estimating MLE standard errors. Given

1112 that the biological parameters enter the likelihood via a nonlinear differential equation,  
 1113 and further the parameters themselves are related to each other nonlinearly, the likeli-  
 1114 hood function can often be difficult to optimize. A hybrid optimization scheme is used  
 1115 to maximize the log likelihood to ensure that a global MLE solution is found. The R  
 1116 package GA [?, ?] is used to run a genetic algorithm to explore parameter space glob-  
 1117 ally. Optimization periodically jumps into the L-BFGS-B local optimizer to refine op-  
 1118 tima within a local mode. The scheme functions by searching globally, with the genetic  
 1119 algorithm, across many initial values for starting the local gradient-based optimizer.  
 1120 The genetic algorithm serves to iteratively improve hot starts for the local gradient-  
 1121 based optimizer. Additionally, optimization is only considered to be converged when  
 1122 the optimum results in an invertible Hessian at the found MLE.

- 1123 • fixed  $M = 0.2$ ,  $a_0 = -1$ ,  $w_\infty = 1$
- 1124 • play with  $\kappa$  and age of selectivity  $a_s$

#### 1125 4.2.5.1 Numbers Indices

While not utilized here, age structured models may commonly model indices as proportional to numbers rather than (or simultaneously to) biomass. When solving the DDE, Eq. (??) points out that the full DDE solution will expose a numbers solution simultaneously with a biomass solution that may be used for these purposes. These solutions are often quite similar since the main driver of process behavior comes from the form of  $R$  which is shared among  $N$  and  $B$ . However, it is common on the west coast of the US that indices derived from commercial fisheries are measured as weights while indices derived from recreational fisheries are often measured as counts. If a numbers index,  $J_t$ , is observed alongside the previously mentioned biomass index, the following likelihood component is often added as a conditionally independent component of the

likelihood,

$$J_t \sim LN(pN_t(\boldsymbol{\theta}, \boldsymbol{\phi}), \tau^2). \quad (4.12)$$

1126  $N_t(\boldsymbol{\theta}, \boldsymbol{\phi})$  is the numbers solution of the DDE system.  $\boldsymbol{\theta}$  and  $\boldsymbol{\phi}$  are the productivity  
1127 and growth parameters shared in common with the biomass component.  $p$  and  $\tau^2$  are  
1128 then the analogous proportionality constant and residual variation of the numbers index  
1129 respectively.

#### 1130 **4.2.6 GP Metamodel**

1131 **point to catch, and LHS design, and Metamodel.**

#### 1132 **4.2.7 Clustering Model Failure**

1133 Considering the behavior observed in Section (??), where  $\frac{F_{MSY}}{M}$  is dramatically un-  
1134 derestimated, it is natural to ask where specifically in RP space we might see this catas-  
1135 trophic failure of the BH model. The structure of RPs under the BH model suggests sev-  
1136 eral natural avenues for forming hypotheses to identify highly misspecified RP regions.  
1137 The single clearest feature to identify are cases where  $\frac{F_{MSY}}{M}$  is heavily under-estimated.  
1138 Here this idea is expressed by a hypothesis testing inspired framework that uses the GP  
1139 metamodel to propagate estimate uncertainty across the simulated space of misspec-  
1140 ified BH RPs. This allows for a rejection threshold (against the null hypothesis that  
1141 BH RP estimates are unbiased) to be derived in terms of the GP predictive structures  
1142 to define a classifier for identifying where BH inference breaks down broadly over RP  
1143 space.

1144 Recall that the metamodel models MLE estimates of  $\log(F_{MSY})$  under the misspec-  
 1145 ified BH model. Thus, for a given set of RPs,  $\mathbf{x}$ , of the BH metamodeled quantity is  
 1146 given by kriging prediction as  $N(\hat{y}(\mathbf{x}), \hat{\sigma}^2(\mathbf{x}))$ , where  $\hat{y}(\mathbf{x})$  is the kriging mean (as pre-  
 1147 viously described in Eq. (??)) and  $\hat{\sigma}^2(\mathbf{x})$  provides estimate uncertainty via the kriging  
 1148 predictive variance given by,

$$\hat{\sigma}^2(\mathbf{x}) = \mathbf{R}(\mathbf{x}, \mathbf{x}) - \mathbf{r}(\mathbf{x})' \mathbf{R}_\ell^{-1} \mathbf{r}(\mathbf{x}). \quad (4.13)$$

1149 Model failure with respect to estimating  $\frac{F_{MSY}}{M}$  under the BH model is measured by  
 1150 the percent error as previously described in Section (??). When the BH model estimates  
 1151  $\frac{F_{MSY}}{M}$  well the percent error is expected to be small in the following sense,

$$\frac{\frac{F_{MSY}}{M} - \frac{\hat{F}_{MSY}}{M}}{\frac{F_{MSY}}{M}} < P. \quad (4.14)$$

1152  $P$  defines the extent of model failure on the scale of percent error. For measuring  
 1153 catastrophic model failure  $P$  was chosen to be 0.5, but smaller values of  $P$  may be  
 1154 chosen to emphasize regions of more subtle model failure. Thus when the percent  
 1155 error is statistically greater than  $P$  the notion that the BH model estimates  $\frac{F_{MSY}}{M}$  well (in  
 1156  $P$ -sense) is rejected.

1157 For statistical evaluation, it is convenient to rearrange Eq. (??) as  $\hat{F}_{MSY} > (1 - P)F_{MSY}$ .  
 1158  $\hat{F}_{MSY}$  is then distributed as  $LN(\hat{y}(\mathbf{x}), \hat{\sigma}^2(\mathbf{x}))$ , and the rejection region is then defined  
 1159 as the RP's for which the 5<sup>th</sup> percentile from the Log-normal distribution falls below  
 1160  $(1 - P)F_{MSY}$ .



## 4.3 Results

### Biological Regeim $\text{corr}(a_s, \kappa) < 0$

Figure (??) shows three hypothetical individual-growth/maturity curves that span a wide range of RPs. As seen in Figure (??), the larger values of  $w(a_s)$  correspond to larger recruits relative to maximum size. This leaves little growth to be evaluated by the biomass dynamics equations; the red curve demonstrates the simple (no growth) production model limit ( $a_s \rightarrow 0$  and  $\kappa \rightarrow \infty$ ). The cases shown with smaller  $w(a_s)$  values (blue and purple curves) correspond to slower growth behaviors. The blue curve, where  $a_s = 2$  and  $\kappa = 0.1$ , emphasizes the effect of growth on the biomass dynamics most among these examples.

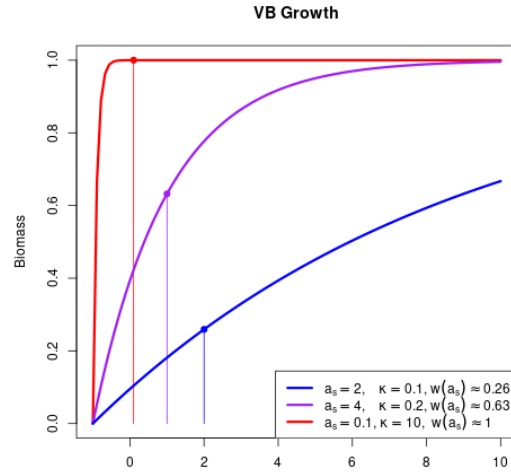


Figure 4.3: Three hypothetical individual-growth curves, showing  $w(a_s)$  on each curve.

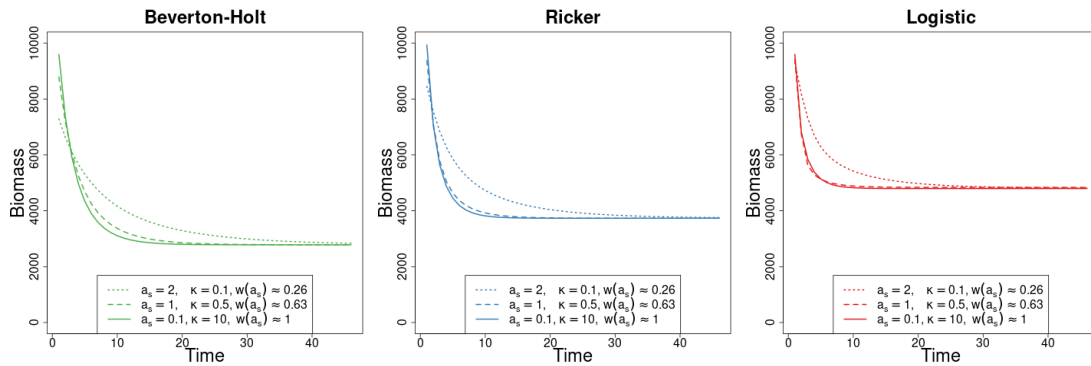


Figure 4.4: Biomass dynamics of BH (*left*), Ricker (*center*), and Logistic (*right*) delay differential models in the low contrast simulation setting. In all cases  $\alpha = 1.2$  and  $\beta$  is chosen so that each model shares the same  $B_{MSY}$  within each given  $\gamma$ .

Figure (??) demonstrates a range of biomass dynamics that the Schnute delay model can display under a spectrum of growth behaviors with fishing held consistent at  $F_{MSY}$ . The three special cases of  $\gamma = -1$  (BH),  $\gamma \rightarrow 0$  (Ricker), and  $\gamma = 1$  (Logistic) recruitment are shown in each of the above growth configurations.

Figure (??) shows the range of RPs that can be modeled with each of the BH, Ricker, and Logistic recruitments over the spectrum of individual-growth/maturity models simulated here. Notice for smaller values of  $w(a_s)$  the further the RP curve lies from the simple production model, and each recruitment model reacts slightly differently under each of the given growth parameters. The Ricker and BH RP-spaces are qualitatively similar in shape with smaller values of  $w(a_s)$  decreasing  $\frac{B_{MSY}}{B_0}$  relative to the simple production model setting. The Logistic model on the other hand increases  $\frac{B_{MSY}}{B_0}$  relative to the simple production model setting as smaller values of  $w(a_s)$  decreases. It is also worth noting that the Ricker model's RPs are much less influenced by growth parameters as compared with that of the BH or Logistic model.

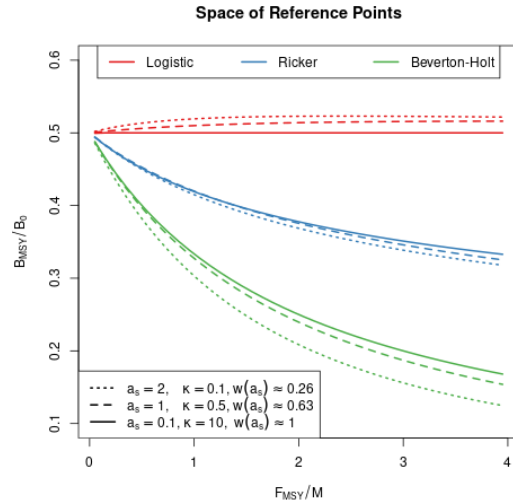


Figure 4.5: Restricted RP-space under each recruitment models, with each growth curve.

### 4.3.1 Simple Production Model Limit

Under the delay differential's limiting simple production model ( $a_s = 0.1$  and  $\kappa = 10$ ), the expectation is that RP inference should be identical to that of the model seen in Chapter (3). By way of verifying this equivalence, Figure (??) demonstrates a virtually identical pattern of RP biases as previously seen in Figures (3.7) and (3.8) (under both of the high and low contrast settings).

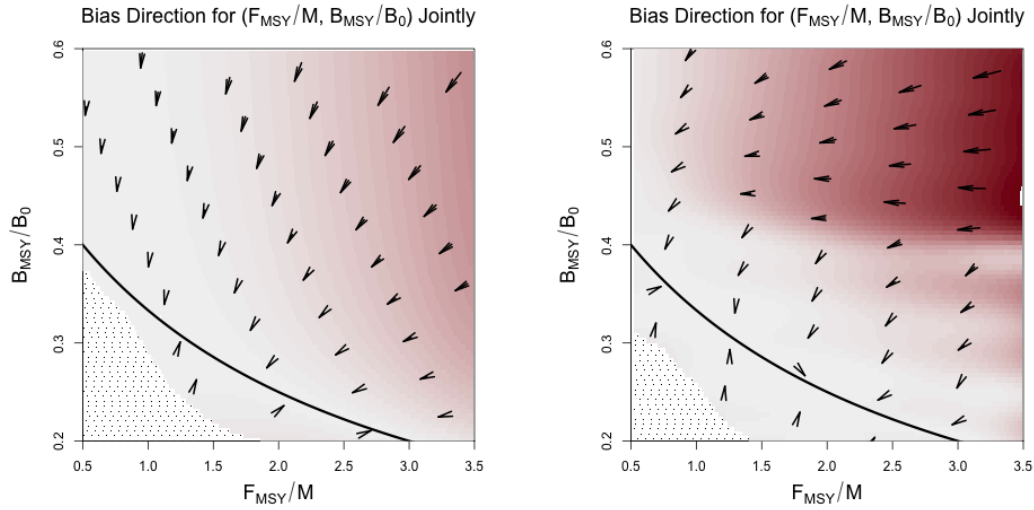


Figure 4.6: RP mapping of BH delay model fit to Schnute delay data under the simple (no growth) production model limit. *left* : High contrast simulation. *Right* : Low contrast simulation.

Indeed in the high contrast setting, Figure (??, *left*) shows how the BH model induces the same pattern of bias as seen in Chapter (3). There is bias in both RPs (in accordance with the  $\frac{B^*}{B(0)} = \frac{1}{F^*/M+2}$  RP-set) so as to produce a nearly minimal distance mapping of RPs onto the constrained BH set of RPs. Similarly, in the low contrast setting, Figure (??, *right*) again shows the same two regimens pattern of RP inference. Firstly, there is a region of relatively small model misspecification where the minimal distance mapping is preserved. Secondly, as model misspecification becomes greater (around the Ricker set)  $\frac{F^*}{M}$  begins to be sharply underestimated. Above this break point

1212 in RP estimation inference appears to be driven toward the trivial RP  $\frac{F^*}{M} = 0, \frac{B^*}{B(0)} = 0.5$   
1213 that is shared in common among all of the two-parameter models described here.

1214 These results confirm that the theoretical limiting dynamics do indeed replicate  
1215 expected RP inference patterns as previously observed in Chapter (3).

### 1216 4.3.2 Moderate Growth

1217 Moving past the simple production model, other values of  $a_s$  and  $\kappa$  provide a probe  
1218 into the effects individual growth dynamics may have on RP inference. Individual  
1219 growth is a multifaceted phenomena that is not easily reduced to a single number, but  
1220 for the purposes of this model  $w(a_s)$  serves as a decent proxy for the extent of the model  
1221 dynamics that are due to individual growth. This follows from the intuition that individ-  
1222 uals maturing at a smaller fraction of  $w_\infty$  demonstrate the dynamics of growth during  
1223 an observable (to the model) phase rather than growth occurring prior to selection.

1224 That said,  $w(a_s)$  is not a one-to-one map of  $\kappa$  and  $a_s$ . A level curve of  $w(a_s; \kappa) = c$   
1225 is attained by increasing the value of  $a_s$  and decreasing  $\kappa$  correspondingly, or vice versa.  
1226 The case where  $a_s = 1$  and  $\kappa = 0.5$  (resulting in  $w(a_s) \approx 0.6$ ) represents a reasonable  
1227 biological example of moderate growth. Similar examples of the  $w(a_s) = 0.6$  level  
1228 curve result in much larger lags (discussed in Section (??)) or larger  $\kappa$ 's which quickly  
1229 tend toward behaviors previously described in the simple production model setting.

1230 The RP mappings seen in Figure (??) show very similar RP mappings to that of  
1231 the simple production model, with the biggest differences occurring around the location  
1232 of the break point where the low contrast model begins to dramatically underestimate  
1233  $\frac{F^*}{M}$ . In the high contrast simulation setting Figure (??; *left*), the RP mappings again  
1234 demonstrate a nearly identical minimal distance mapping of RPs onto the constrained  
1235 BH RP set. In the low contrast setting Figure (??; *right*) a very similar two regiem  
1236 pattern of RP inference is observed, however the location of the break between these

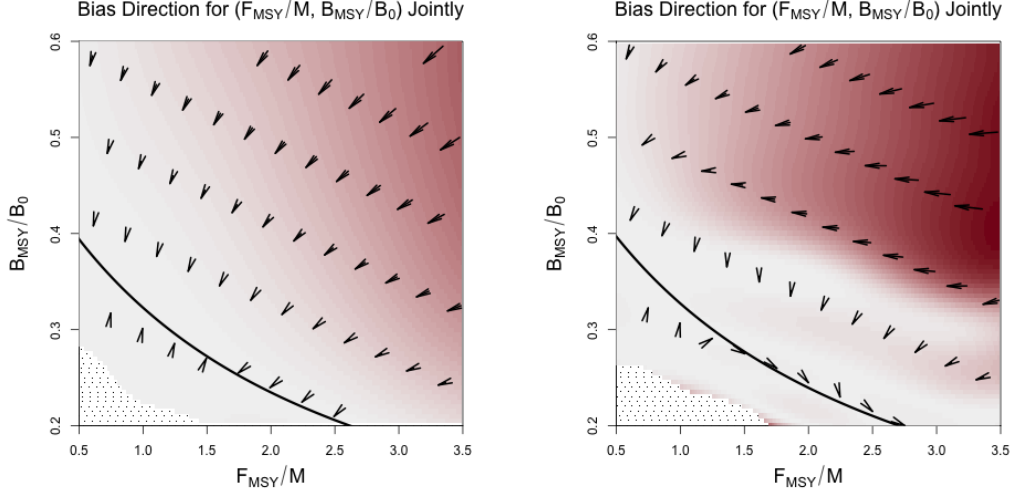


Figure 4.7: RP mapping of BH delay model fit to Schnute delay data under moderate growth ( $a_s = 1$  and  $\kappa = 0.5$ ). *Left* : High contrast simulation. *Right* : Low contrast simulation.

regiems appears at lower values of  $\frac{B^*}{B(0)}$ . In this moderate growth setting the break point  
occures around values of  $\frac{B^*}{B(0)}$  just below 0.4 as opposed to the simple production model  
the break point occurs at  $\frac{B^*}{B(0)}$  just above 0.4.

### 4.3.3 Emphatic Growth Dynamics

The emphatic growth setting simulated here fixes  $a_s = 2$  and  $\kappa = 0.1$ , to simulate a  
species that grows quite slowly and matures into the reproducing stock at a relatively  
early age. This combination has the effect of exaggerating the components of the model  
dynamics which are related to individual growth since individuals recruit at a small size  
and slowly grow over the extent of the modeled period.

The slow growth of these dynamics oppose the simple production model setting in  
the sense that they move the constrained RP set a large distance (largest among the  
spectrum of decreasing  $w(a_s)$  populations simulated here) away from the  $\frac{1}{x+2}$  limiting  
case. It is interesting to note that this is true for all of the two parameter constrained

constrained RP sets as seen in Figure (??).

Despite the heavily growth influenced driven biomass dynamics in this setting, the RP mappings seen in Figure (??) obviously bare a huge resemblance to the previously seen RP mappings. Again the biggest differences in the RP mappings occur around the location of the break point where the low contrast model begins to dramatically underestimate  $\frac{F^*}{M}$ . In this low contrast setting the break point in RP estimation occurs

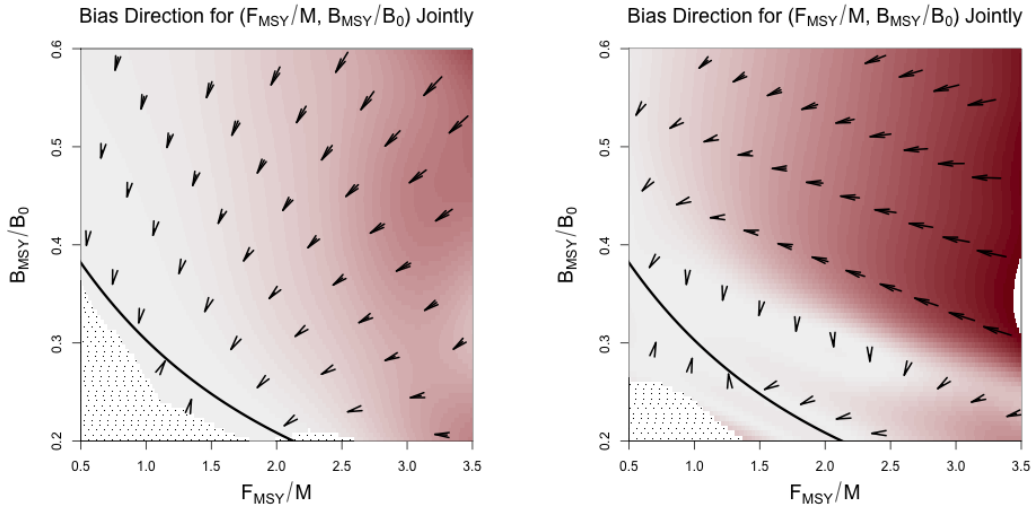


Figure 4.8: RP mapping of BH delay model fit to Schnute delay data under dramatic growth ( $a_s = 2$  and  $\kappa = 0.1$ ). *Left* : High contrast simulation. *Right* : Low contrast simulation.

around values of  $\frac{B^*}{B(0)}$  well below 0.4 with the behaviour extending as far down as  $\frac{B^*}{B(0)} = 0.3$ . This regiem shift occurs well below that of the Ricker set, as initially observed in the production model setting. This reduced range of acceptable RP inference indicates that under increasingly emphatic growth the model misspecification issue of the BH model becomes an increasingly brittle assumption with respect of RPs.

Interestingly this pattern only follows for the low contrast setting. In the high contrast setting inference returns to a pattern resmbleing the minimal distance mapping onto BH RP set. Further pointing to the importance of contrast for informing these

models.

#### 4.3.4 Clustering Catastrophic Model Failure

Figure (??) shows the rejection thresholds for the low contrast simulations of each of the emphatic, moderate, and no growth settings. The dark lines represent the rejection threshold with a false positive rate of about 15%, and the light shaded regions show how the rejection threshold changes as the false positive rate ranges from 50% to 2.25%. When applied to the high contrast simulations the rejection threshold falls outside of the simulated RP range as expected by inspection of the high contrast RP mappings.

Notice in Figure (??) that the rejection threshold is subject to two axes of sensitivity. Firstly, for each simulated growth the rejection threshold is more sensitive for small values of  $\frac{F_{MSY}}{M}$  than for large values. This is a natural result since discerning  $\hat{y}(x)$  below the minimum simulated RP becomes more difficult when the data are truly generated near the minimum simulated  $\frac{F_{MSY}}{M}$ . For large  $\frac{F_{MSY}}{M}$  the minimum distance mapping results in  $\hat{y}(x)$  well above the minimum simulated RP but for

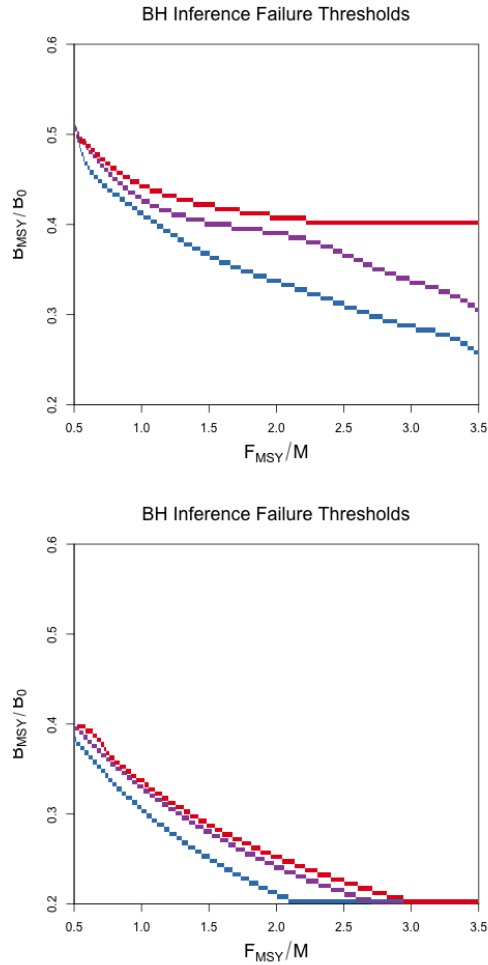


Figure 4.9: BH RP estimation failure thresholds with increasingly emphatic individual growth dynamics.

1290 small  $\frac{F_{MSY}}{M}$  even the minimum distance mapping may be close to the rejection threshold.

1291       The second axis of sensitivity is between individual growth simulations. The no  
1292 growth setting produces a very clear threshold of model failure, while the failure thresh-  
1293 old for emphatic growth is much more varied, especially near the minimum simulated  
1294  $\frac{F_{MSY}}{M}$ . This is largely due to the increased RP estimate uncertainty as growth becomes  
1295 more emphatic in the dynamics.

1296       Model misspecification of the BH model is compounded for the more emphatic  
1297 growth settings as recruitment can interact with growth dynamics to produce unique  
1298 behaviors as exemplified in Section (??).



### 4.3.5 Oscillatory Growth Influence

While the above patterns of RP estimation follow for biological regimens of the  $w(a_s; \kappa) = c$  level curve, as  $a_s$  increases an oscillatory regimen also exists within these dynamics. While RP estimation behaves similarly in this oscillatory regimen there are unique features in this setting that are not present in the more biological regimens. Below consider the oscillatory example of a logistic delay model with  $a_s = 10$  fixing fishing at  $F_{MSY}$ .

Figure (??) demonstrates the mechanism of how these oscillatory dynamics form. Oscillatory dynamics appear when fishing pushes biomass past  $B_{MSY}$  within the lagged  $a_s$  window of recruitment. The delay model assumes that biomass is fixed in equilibrium at  $B_0$ , for  $t \leq 0$ . Therefore in the green region of the biomass series,  $0 < t < 10$ , the population recruits at  $R(B_0)$ . Figure (??) shows that in this initial period  $R(B_0)$  results in zero yield for that period, and biomass falls as a result.

Once  $t$  exceeds  $a_s$ , the lagged recruitment refers to the integrated biomass series to evaluate recruitment based on  $R(B_{t-a_s})$ . The red region of the biomass series is the result of yield over the initial green biomasses. Figure (??) shows that the yield over the green biomass series first increases, as biomass approaches  $B_{MSY}$  and then decreases as biomass passes  $B_{MSY}$ . This creates the local maximum in the red biomass series.

Furthermore, the blue region of the biomass series is then based on yield over the red biomasses. Notice that since the red biomasses first increase and then decrease, yield increases as the red biomass increases toward  $B_{MSY}$ , and yield subsequently decreases following the descending leg of the red biomass series. This yield pattern carries the oscillation of the red biomass region forward into the blue region.

This process of biomass oscillation carries on in this manner nonetheless approaching equilibrium at  $B_{MSY}$ . Equilibrium is reached in an oscillatory manner setoff by the green biomass series crossing over from above  $B_{MSY}$  to below it. The example shown in Figure (??) exemplifies the oscillatory phenomena simulated here, but the mechanism

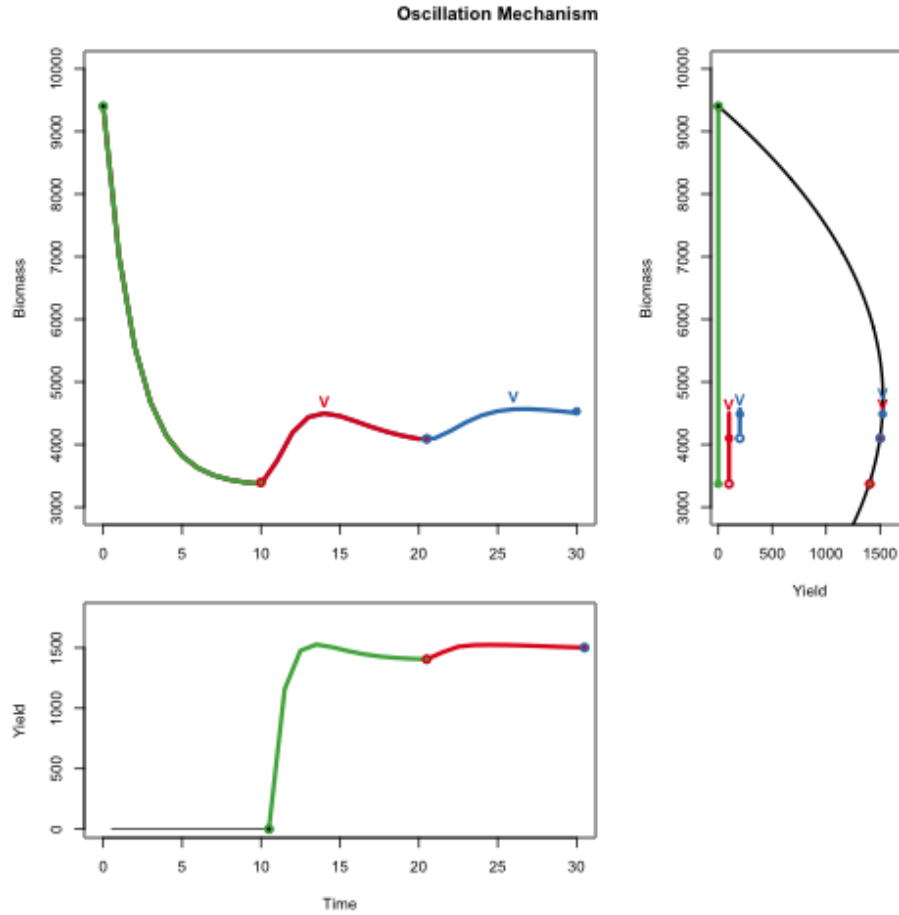


Figure 4.10: *top left* : Logistic biomass over 30 epochs of time with  $a_s = 10$ . Green, red, and blue colors indicate three 10 epoch long windows of biomass. v indicates local biomass oscillation maxima. *top right* : Yield plotted over the range of biomasses shown. The biomass range of each 10 epoch window is shown in the vertical colored lines. *bottom left* : Yield plotted through time. Colors correspond to the lagged biomass region that results in the evaluated yield. The black horizontal line demonstrates the pre-model assumption of biomass fixed at  $B_0$ .

1326 that produces these oscillations may occur with other forms of recruitment outside of lo-  
 1327 gistic recruitment whenever fishing cases biomass to cross over  $B_{MSY}$  within the lagged  
 1328 recruitment window.

### 4.3.5.1 RP Estimation

Statistical inference in the oscillatory regiem can be challenging. Depending on the parameters inferred, the likelihood can have multiple local modes which require global optimization techniques to distiguish. Furthermore, parameter estimation is more uncertain in this setting as the likelihood may confuse oscillations with residual noise.

Figure (??) shows the BH RP mapping fixing  $w(10;0.1) \approx 0.6$  in the high contrast simulation setting. This places the dynamics firmly in the ocillatory regiem, but the high contrast setting provides significant information for inferring recruitment parameters.

Interestingly in this high contrast setting, a very similar two regiem pattern of RP inference is observed as previously seen in low contrast settings. That said the boundary between the regiems in this setting is much smoother and the location of the break between these regiems appears around higher values of  $\frac{B^*}{\bar{B}(0)}$ .

This higher  $\frac{B^*}{\bar{B}(0)}$  break point, hovering around 0.5, is consistent with the mecha-

nism which induces ocillation. Starting the biomass at  $\bar{B}(0)$  in the ocillatory regiem, increased  $\frac{B^*}{\bar{B}(0)}$  will tend to exasterbate oscillatory behavior by increasing  $B_{MSY}$  so that biomass is more easily pushed past  $B_{MSY}$  within the initial lagged as window of recruitment. This produces more dramatic oscillations in the higher  $\frac{B^*}{\bar{B}(0)}$  region of RP space.

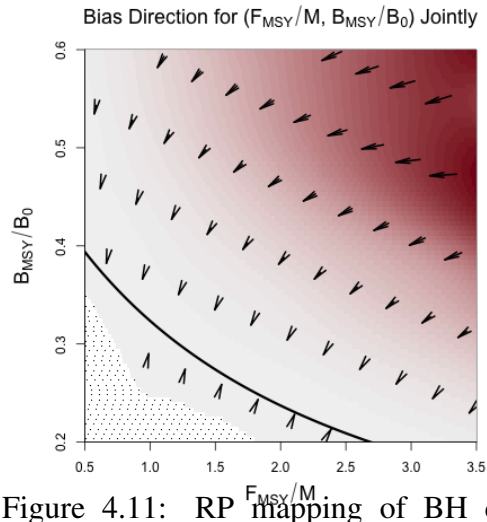


Figure 4.11: RP mapping of BH delay model fit to high contrast Schnute delay data under oscillatory growth ( $a_s = 10$  and  $\kappa = 0.1$ ).

1354 The fitted BH model does not pro-  
 1355 duce significant oscillations because un-  
 1356 der the BH model  $\frac{B^*}{B(0)}$  is constrained be-  
 1357 low 0.5 with the majority of the simu-  
 1358 lation BH  $\frac{B^*}{B(0)}$  RPs falling between 0.4  
 1359 and 0.2. Therefore, the fitted BH model  
 1360 will not tend to push biomass past  $B_{MSY}$   
 1361 and thus is incapable of modeling oscilla-  
 1362 tory biomass series. Figure (??) shows a  
 1363 subset of example BH fits, which demon-  
 1364 strates the limited oscillatory capacity of  
 1365 the BH fits. Furthermore, since the BH model has a limited oscillatory capacity in this  
 1366 setting, the BH model tends to explain the oscillations with artificailly high residual  
 1367 variation and artificailly low steepness focusing on overly simplistic trends in the data.

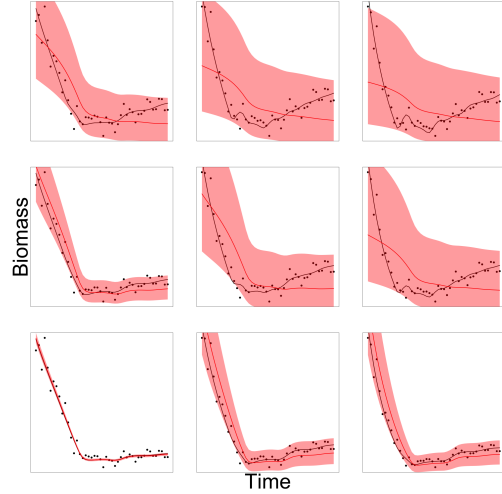


Figure 4.12: Example BH fits (*red*) to Schnute data (*black*). Each example plot is arranged to mirror its location in RP space.

#### 1368 4.3.5.2 Estimating More

1369 Figure (??) shows a subset of exam-  
 1370 ple model fits broadly over RP space.  
 1371 Model fits are shown both under the two-  
 1372 parameter BH model as well as under  
 1373 the three parameter Schnute model, each  
 1374 model estimating all of its recruitment pa-  
 1375 rameters as well as the growth and matu-  
 1376 rity parameters  $\kappa$  and  $a_s$ . Notice that the  
 1377 BH model, even when additionally esti-  
 1378 mating  $\kappa$  and  $a_s$ , does not gain the flexi-  
 1379 bility to properly model Schnute data.

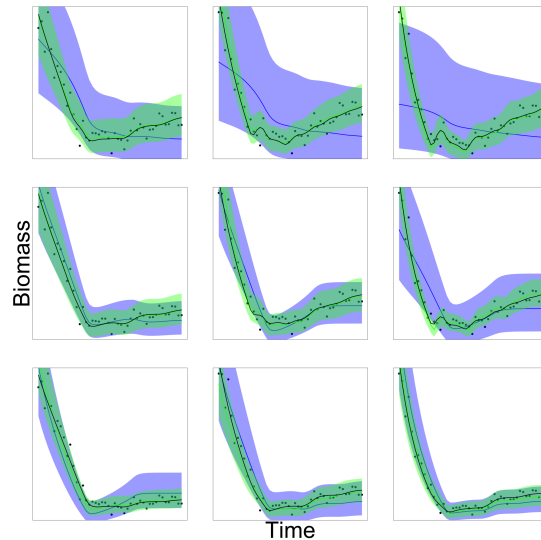


Figure 4.13:  $\kappa$  and  $a_s$  estimation under BH (*blue*) and Schnute (*green*) fits to Schnute data (*black*) arranged to mirror RP space.

1380       The lack of oscillatory dynamics pro-  
1381       duced by the BH model causes the mis-  
1382       specified BH fits in Figure (??) to largely  
1383       estimates  $\kappa$  and  $a_s$  so as to approximate the production model limiting case. The fitted  
1384       Schnute model can produce the oscillatory dynamics and thus the information in the os-  
1385       cillatory data well inform estimates of  $\kappa$  and  $a_s$  under the Schnute model. Furthermore,  
1386       the Schnute model has no issue learning its  $\gamma$  parameter.

1387       While Statistical inference in the oscillatory regiem can be challenging in the highly  
1388       constrained BH model, the Schnute model can easily estimate its extra  $\gamma$  parameter. The  
1389       flexibility of estimating  $\gamma$  simplifies inference by correctly specifying RPs, and also by  
1390       opening up the model dynamics to reveal additional information about  $\kappa$  and  $a_s$  in the  
1391       data.

## 1392 4.4 Discussion

- 1393 • break point decreases with growth
- 1394 • inference becomes more brittle with more dramatic growth.
  - 1395 – interaction between assumed form of growth and stock recruitment.
  - 1396 – low-side steepness bias masks oscillatory/shock patterns induced by growth
  - 1397 and maturity parameters
- 1398 • misspecified BH prevents learning growth
- 1399 • increasing growth accelerates model misspecification
- 1400 • statistical evidence of minimum distance mapping within acceptable region, al-
- 1401 though float idea of PT-like pattern as BH set flattens. (explaining perturbations)

## 1402 4.5 old ideas

- 1403 • show production model limit (contrast
  - 1404 –  $a_s \rightarrow 0$ : instant maturity
  - 1405 –  $\kappa \rightarrow \infty$ : recruit as an adult ()
- 1406 • describe second order shapes of growth/maturity (and cause)
  - 1407 – weight of recruits  $\Rightarrow$  scaling biomass ( $q$ ,  $\beta$ , and  $w_\infty$ )
  - 1408 –
- 1409 • describe RP bias
- 1410 • flat

## <sup>1411</sup> **Chapter 5**

## <sup>1412</sup> **Conclusion**

## 1413 **Appendix A**

### 1414 **Inverting $\frac{B^*}{\bar{B}(0)}$ and $\gamma$ for the PT Model**



Let  $\zeta = \frac{B^*}{B(0)}$ .

$$\zeta = \left(\frac{1}{\gamma}\right)^{\frac{1}{\gamma-1}}$$

$$\zeta = \gamma \zeta^\gamma$$

$$\zeta = \gamma e^{\gamma \log(\zeta)}$$

$$\zeta \log(\zeta) = \gamma \log(\zeta) e^{\gamma \log(\zeta)}$$

The Lambert product logarithm,  $W$ , is defined as the inverse function of  $z = xe^x$  such that  $x = W(z)$ . Applying this definition allows for the isolation of  $\gamma$ .

$$\begin{aligned} \gamma \log(\zeta) &= W(\zeta \log(\zeta)) \\ \gamma &= \frac{W(\zeta \log(\zeta))}{\log(\zeta)} \end{aligned} \tag{A.1}$$

1415 The Lambert product logarithm is a multivalued function with a branch point at  $-\frac{1}{e}$ .  
 1416 The principal branch,  $W_0(z)$ , is defined on  $z \in (-\frac{1}{e}, \infty)$ , and the lower branch,  $W_{-1}(z)$ ,  
 1417 is defined on  $z \in (-\frac{1}{e}, 0)$ . Taken individually, each respective branch is analytic, but  
 1418 cannot be expressed in terms of elementary functions.

1419 When  $\zeta \in (0, \frac{1}{e})$  the solution of interest in Eq. (2.10) comes from  $W_0$ . When  $\zeta \rightarrow \frac{1}{e}$ ,  
 1420 the Fox Model emerges as  $\gamma \rightarrow 1$ . When  $\zeta \in (\frac{1}{e}, 1)$  the solution of interest comes from  
 1421  $W_{-1}$ . For the use case presented here, Eq. (2.10) is to be interpreted as,

$$\gamma = \begin{cases} \frac{W_0(\zeta \log(\zeta))}{\log(\zeta)} & \zeta \in (0, \frac{1}{e}) \\ \frac{W_{-1}(\zeta \log(\zeta))}{\log(\zeta)} & \zeta \in (\frac{1}{e}, 1) \end{cases}. \tag{A.2}$$

## <sup>1422</sup> **Appendix B**

### <sup>1423</sup> **Relation to $F_{SPR}$ Proxy**

1424 • Define  $F_{MSY}$  Proxy  $F_{SPR_x}$

1425 • Define  $\frac{B_{MSY}}{B_0}$  Proxy  $B_y$

1426 • List management targets for RF, GF, FF

	$B_y$	$SPR_x$	$\left[\frac{B_{MSY}}{B_0}\right]_{BH}$	$\left[\frac{F_{MSY}}{M}\right]_{BH} (F Only)$
RF	$y = 0.40$	$x = 0.50$	0.29	1.45 (0.29)
GF	$y = 0.40$	$x = 0.45$	0.22	2.46 (0.49)
FF	$y = 0.25$	$x = 0.30$	0.21	2.87 (0.57)

1428 • Show BH calculation only hits target for  $\frac{\alpha}{M} = 6$ ; target cannot equal MSY.

1429 • Show general  $\alpha$ - $\gamma$  proxy relation under Schnute.

1430  $B_0$  given by Eq. (3.4).  $R_0$  is given by evaluating  $R(B_0; \theta)$ .

$$R_0 = \frac{M}{\gamma\beta} \left( 1 - \left( \frac{M}{\alpha} \right)^\gamma \right) \quad (B.1)$$

$$F_{SPR_x} = \frac{R_0}{xB_0} - M = M \left( \frac{1}{x} - 1 \right) \quad (B.2)$$

1431 Evaluating  $\frac{B_{MSY}}{B_0}$  Eq.(3.5) at  $F_{SPR_x}$ . Solving for the compensation ratio  $\frac{\alpha}{M}$  gives,

$$\frac{\alpha}{M} = \left[ \frac{\frac{1}{x^\gamma} - y}{1 - y} \right]^{1/\gamma} \quad (B.3)$$

1432 • Show general  $\alpha$ - $\gamma$  MSY relation under Schnute.

1433 Reference  $\alpha$  Eq.(3.9) from text in  $F_{MSY}$ .

1434 When  $F_{MSY} = F_{SPR_x}$  substitute in Eq.(??)

$$\frac{\alpha}{M} = \frac{1}{x} \left( 1 + \gamma(1 - x) \right)^{1/\gamma} \quad (B.4)$$

1435 • Show single  $(\alpha, \gamma)$  pair to hit both proxy and MSY.

1436

Equate Eqs. (??) and (??)

$$\left[ \frac{\frac{1}{x^\gamma} - y}{1 - y} \right]^{1/\gamma} = \frac{1}{x} \left( 1 + \gamma(1 - x) \right)^{1/\gamma} \quad (\text{B.5})$$

$$1 - yx^\gamma = \left( 1 + \gamma(1 - x) \right) (1 - y) \quad (\text{B.6})$$

$$1 = \left[ 1 - \gamma \frac{(1 - x)(1 - y)}{y} \right] x^{-\gamma} \quad (\text{B.7})$$

1437

$$r(x, y) = \frac{y}{(1-x)(1-y)}$$

$$r(x, y) = \left( r(x, y) - \gamma \right) x^{-\gamma} \quad (\text{B.8})$$

1438

Recall the Lambert product logarithm,  $W$ , is defined as the inverse function of

1439

$z = xe^x$  such that  $x = W(z)$ . Isolating  $\gamma$  requires that the above expression be

1440

placed into  $xe^x$  form to apply the definition of  $W$ .

$$r(x, y)x^{r(x, y)} = \left( r(x, y) - \gamma \right) x^{r(x, y) - \gamma} \quad (\text{B.9})$$

$$r(x, y)x^{r(x, y)} \log(x) = \left( r(x, y) - \gamma \right) \log(x) e^{\left( r(x, y) - \gamma \right) \log(x)} \quad (\text{B.10})$$

$$W_{-1} \left( r(x, y)x^{r(x, y)} \log(x) \right) = \left( r(x, y) - \gamma \right) \log(x) \quad (\text{B.11})$$

$$\gamma = r(x, y) - \frac{W_{-1} \left( r(x, y)x^{r(x, y)} \log(x) \right)}{\log(x)} \quad (\text{B.12})$$

1441

The solution of interest for  $\gamma$  in terms of only the proxy values comes from  $W_{-1}$ .

1442

To complete the point  $(\alpha, \gamma)$  in terms of only proxy values  $\alpha$  is given by substituting  $\gamma$  from Eq.(??) into either of Eqs. (??) or (??).

1443

1444

- a few pics demonstrating the result

## <sup>1445</sup> **Appendix C**

### <sup>1446</sup> **Delay Differential Replacement Line**

1447 The replacement line is the rate of productivity which exactly balances biomass loss  
 1448 in the absence of fishing. In the simple production model, productivity must simply  
 1449 balance biomass loss due to  $M$ . Thus when  $R(B; \theta) > MB$  there will be some surplus  
 1450 productivity to enable fishing.

In the delay model, productivity is complicated by biomass changing, both with the recruitment of young into the reproducing population, as well as biomass accumulation due to the growth of existing individuals in the population. To derive the replacement line in the case of the delay model the equilibrium equations in the absence of fishing are considered and the  $R(B)$  that this implies is then isolated.

$$0 = \frac{dB}{dt} = w(a_s)R(B) + \kappa[w_\infty N - B] - MB \quad (\text{C.1})$$

$$0 = \frac{dN}{dt} = R(B) - MN. \quad (\text{C.2})$$

Eq(??) quickly gives  $\bar{N} = R(B)/M$ . Substituting this equilibrium value into Eq(??) to rewrite  $N$  in terms of  $B$ ,

$$0 = w(a_s)R(B) + \kappa \left[ w_\infty \frac{R(B)}{M} - B \right] - MB. \quad (\text{C.3})$$

Collecting like terms,

$$R(B) \left[ w(a_s) + \frac{\kappa w_\infty}{M} \right] = [M + \kappa] B. \quad (\text{C.4})$$

Finally solving for  $R(B)$ , and simplifying, gives the equation of the replacement line as,

$$R(B) = \left[ \frac{M(M + \kappa)}{w(a_s)M + \kappa w_\infty} \right] B. \quad (\text{C.5})$$